DAMAGE ASSESSMENT METHODOLOGY FOR FLOODS
Short report

Center for Urban Water

Metro Colombo Urban Development Project
Ministry of Urban Development, Water Supply and Housing Facilities

Wing C, 10th Floor, Sethsiripaya Stage II, Battaramulla, Sri Lanka

DAMAGE ASSESSMENT METHODOLOGY FOR FLOODS

Short report

Center for Urban Water

Metro Colombo Urban Development Project
Ministry of Urban Development, Water Supply and Housing Facilities

Wing C, 10th Floor, Sethsiripaya Stage II, Battaramulla, Sri Lanka

Contents

1. Introduction and the structure of the report 5
1.1. Introduction to the damage assessment report 5
1.2. Structure of the report 5
2. Damage assessment-concept 6
2.1. Introduction 6
3. Derivation of damage functions for structural damage 7
3.1. Data collection 7
3.2. Derivation of damage functions 8
3.3. Damage functions 9
4. Derivation of damage functions for content damage 10
4.1. Data Collection and validation 10
4.2. Analysis of data 10
4.3. Derivation of the damage indices and damage functions 12
4.4. Short discussion 14
5. Damage assessment-implementation methodology 14
5.1. Damage calculation (vector format) 14
5.2. Damage calculation (raster format) 17
5.3. Comparison of the results given by raster and vector methods 17
5.4. Projecting for the content damage of the residential buildings 18
5.5. Conclusion 19
6. Way forward: Identifying spatial distribution of the economic activities 19
7. Annexes 20
7.1. Annex 01 - Source for structural damage curves 20
7.2. Annex 02 - Annexes on content damage survey 39
7.2.1. Initial composition of the survey locations 39
7.2.2. Surveyed flood depths comparison with the modelled flood depths 39
7.2.3. Damage (LKR/m^2) vs the flood height graphs for the initially identified building types 40
7.3. Annex 03 - Results of the sensitivity analysis 46
7.4. Annex 04 - Comparison between the building properties in the vector format and the raster format 47
7.5. Annex 05 - Calculations for the comparisons between the vector and raster calculations. 54
7.6. Annex 06 - Comparison of three methods to project the content damage of the residential buildings 58

1. Introduction and the structure of the report

1.1. Introduction to the damage assessment report

This report will explain the methods adopted by the Centre for Urban Water (CUrW) for the loss estimations for the simulated past and future flood scenarios. The losses will generally occur in the following aspects.

- Structural damage for buildings (Damages to the building structural elements such as walls/roof)
- Content damage for buildings (Damages to the things inside the building such as sofas/television/refrigerator)
- Damages to the economic activities (Damages occur from not conducting the economic activities such as interruptions to businesses etc.)
- Damages to the prominent infrastructure (such as bridges, roads, culverts, telephone connection points and poles, electrical infrastructure, flood protection structures etc.)
- Damages to the vehicles
- Expenditure for relief (cost borne for the relief requirements of the flood affected people, which is usually born by the relevant governmental authorities such as Disaster Management Centre, National Disaster Relief Services Centre, Municipal councils, Urban Councils and Divisional Secretariats)

There are more types of damages that can be seen in a disaster, which are not easily captured by a physical property, such as the value of a (lost) human life and the extent of a disease outbreak which is due to the cascading effect of the flood event.

Currently, CUrW adopts damage functions prepared for the structural damages and the content damages, which were prepared based on the field surveys carried out by the internal staff of CUrW, in order to calculate the respective damages. At the same time, CUrW seeks opportunities to develop relevant damage curves for the other types of the aforementioned damage categories, through possible partnerships, methodologies and workarounds.

1.2. Structure of the report

The rest of the report will initially explain the concept behind damage assessment, the methodology adopted for the structural damage calculation and the development of the damage curves for the structural damages, the methodology of development of the content damage functions, computational methods for the damage calculation and how CUrW has adopted rapid calculation methodologies for the damage assessments.

2. Damage assessment-concept

2.1. Introduction

Flood damages are assessed considering the flood hazard, exposure of the assets (buildings in this case) and the vulnerability of the exposed structures, by the following formula.

$$Damage = flood\ hazard \times exposure \times vulnerability$$

Here, the flood hazard is expressed by the flood inundation maps, which are often the results of the flood simulation exercises. Flood inundation maps for a particular flood scenario produce two important information: flood extent (area of inundation) and the flood depth at the inundated locations.

Exposure the is the placement of the assets, buildings in this case (if the people at risk is concerned, the exposure would be the peoples' locations). Alongside, the building properties are considered in this stage such as structural properties for the structural damage calculation and the building use categories for the content damage calculations. There are five structural damage categories and nine building use categories considered in assessing damages in this study, as mentioned in the Section 3**Error! Reference source not found.**. These exposure maps are available in the form of vectors (shapefiles), having attributes of building structural fabrication and the building use, for each of the individual buildings.

Vulnerability is contextualized by the vulnerability (damage) functions and the base damage values for each of the building exposure category as discussed in section 3.2**Error! Reference source not found.**. T hese functions can be modelled in the Geographic Information System (GIS) modelling software, in order to calculate the damage for a given flood. Figure 1 demonstrates the concepts of hazard and exposure, where the flood map (hazard) is overlaid with the building footprint layer to show the exposure of the building to the floods.

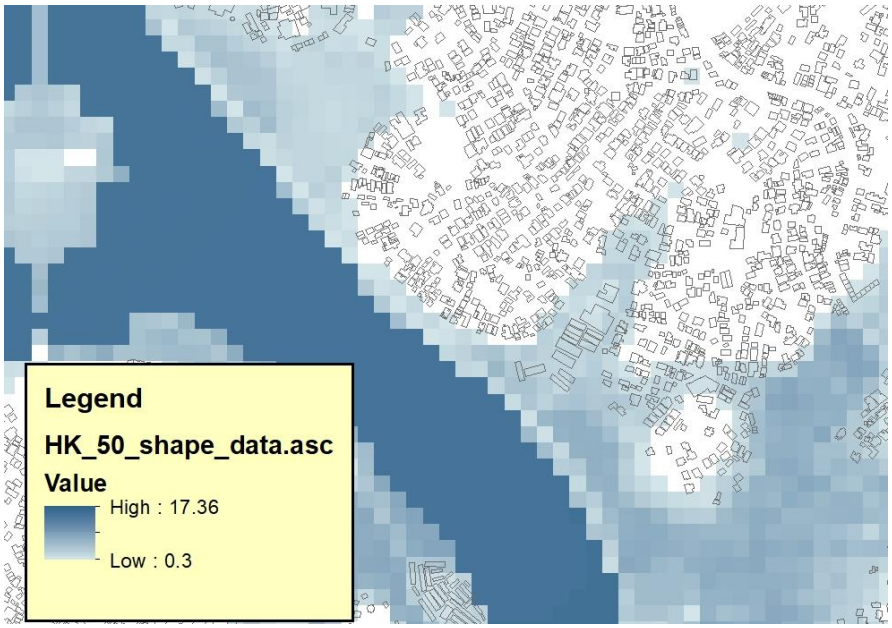

Figure 1. Hazard and Exposure: Hazard is shown by the flood map, where the colour intensity is linked to the flood depth, and the exposure of the buildings in the vicinity is shown by the buildings which have overlapped with the flood map

3. Derivation of damage functions for structural damage

The damage functions for the structural damages are directly drawn from the study from Komolafe et al., 2018, which studies the floods in Sri Lanka for the 2010 floods. Since a comprehensive methodology of derivation of the damage curves and many more information is presented in the aforementioned study, only a summary of the methodology will be explained under this section. The full paper is annexed to this report at Annex 7.1.

3.1. Data collection

For this study, data is collected as a questionnaire survey in the flood affected areas for the recent flood events. There have been 297 respondents, who are mainly adults who have a clear memory of the recent flood events. Data on the replacement cost and the repair cost of the damaged structural items were collected in this survey, alongside with the flood depths and the type of the building in the relevant flood event.

The basic types of the buildings are taken as (A) Unreinforced masonry bearing walls, (B) Concrete frame with unreinforced masonry fill walls, (C) Wooden structures, (D) Commercial buildings as identified by the World Agency of Planetary Monitoring and Earthquake Risk Reduction (WAPMERR) and as documented by United Nations office of Disaster Risk Reduction (UNISDR). Here, it is assumed that the commercial buildings are built with concrete frames and unreinforced masonry walls as well, however the finishes and the furnishes would be different from the general residential buildings. Furthermore, one more building category was identified as (E) Watta, in order to comply to the local conditions. The category Watta usually contain densely populated dwelling units often made with temporary building materials or with unreinforced masonry bearing walls.

3.2. Derivation of damage functions

For each of the building category, the structural damage ratio is calculated taking the total replacement cost and the repair cost in to consideration, in the following manner.

$$Structural\ Damge\ Ratio = \frac{Repair\ Cost}{Replacement\ Cost} \times 100\%$$

It should be noted that the aforementioned repair cost and the replacement costs are calculated per unit area (1 m^2). And then, the structural damage ratio is plotted against the inundation depths of the damaged buildings. Then, based on the following relationship structure, damage functions were derived for the building categories.

$$Damage\ Ratio = C_1 \ln(x) + C_2$$

where C_1 and C_2 are characteristic constants for each building category and x is the flood water depth. The reason to choose the aforementioned structure is due to the logarithm graph shape property of reaching a stable number with the independent variable. In this case the stable number is often the maximum structural damage ratio, and usually it is expected to reach at 3.0 depth level, which is the general ground floor height of a building. The derived damage functions and the damage ratios for structural damage is shown in Figure 2.

At the same time, the base value is calculated for each building category, usually by taking the average replacement cost for a unit area of the building category. This base value is representative of the worth of the building fabric.

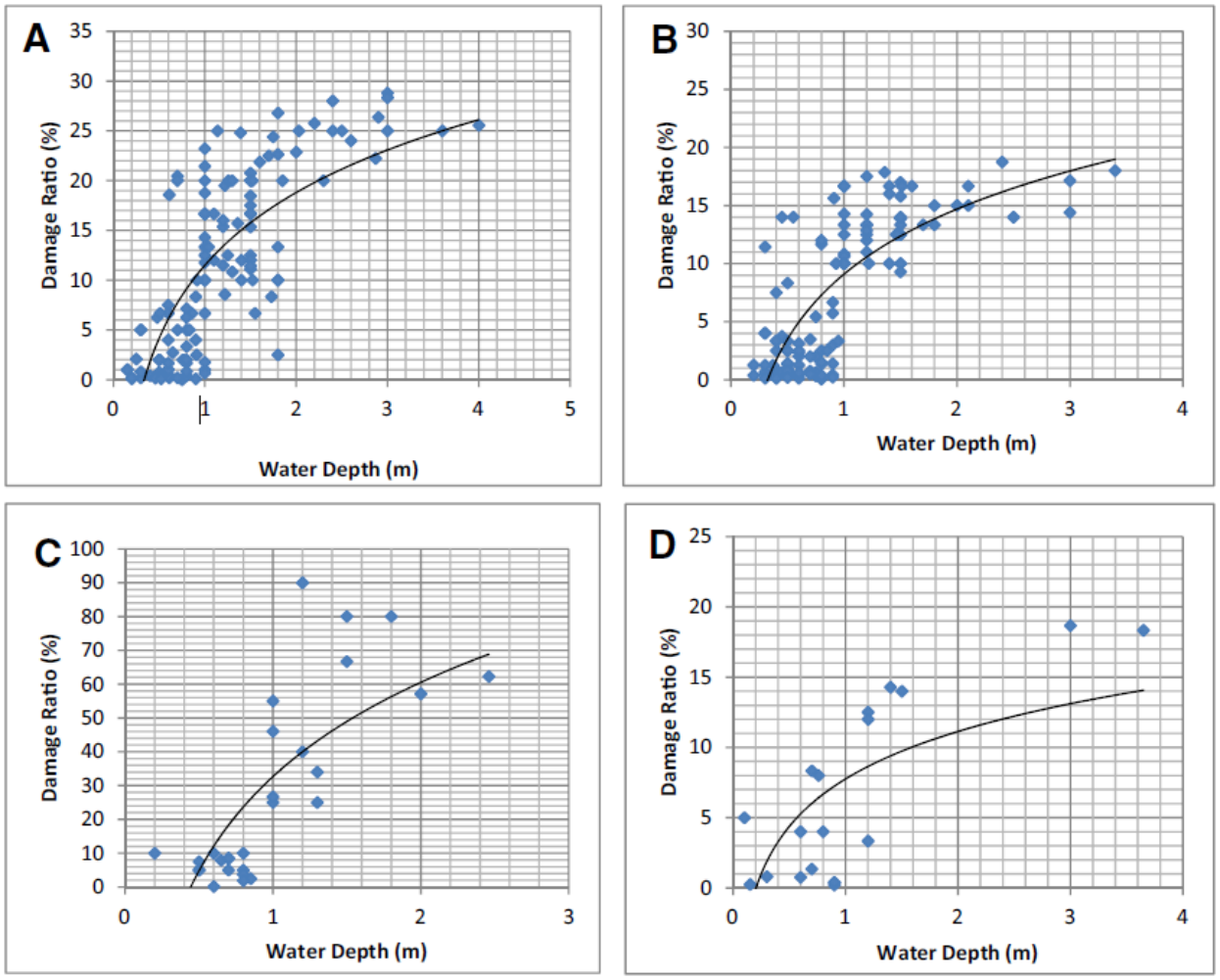

Figure 2. Flood damage curves for A) Residential Unreinforced Masonry (URM), B) Residential concrete frame with unreinforced masonry walls C) Residential wooden structure D) Commercial buildings

3.3. Damage functions

The derived damage functions for the aforementioned building categories are shown below.

Table 1. Damage functions for structural damage

Building category	Base value (LKR/m^2)	Damage functions, D = damage, x = water depth
A - Unreinforced masonry walls (URM)	30,000	$D = 10.55\ln(x) + 11.487$
B - Concrete frame with unreinforced masonry fill walls	80,000	$D = 8.0826\ln(x) + 9.0925$
C - Wooden	6,000	$D = 40.211\ln(x) + 32.656$
D - Commercial building	80,000	$D = 4.875\ln(x) + 7.7563$
Watta	6,000	$D = 10.55\ln(x) + 11.487$

The usage of these damage functions will be explained in the section 5.

4. Derivation of damage functions for content damage

The derivation of damage functions for the content damage is prepared from the scratch, basing a survey done in the flooded areas in the past events. Then based on the surveyed locations and information, 3 main building categories were identified depending on the building use, which is representative of the building content. Next for the identified damage categories, damage functions were derived.

4.1. Data Collection and validation

The field survey was conducted by CUrW interns, who are originally from the University of Ruhuna, covering the aspects of direct-damages for the content of the commercial and industrial buildings, for the flood events in 2010, 2016, 2017 and 2018. The survey locations were chosen in a manner that most of the locations had had damages from multiple flood events. This was identified by the flood simulations for the past flood events for the Metro Colombo Urban Region, and by overlapping the resultant flood map with the building layer map in CUrW.

Since the data collected from the survey is required to be validated, the variables that are required to be validated were identified initially. Since the end goal is to develop depth damage curves with a normalization method for damages, it was identified that the flood inundation depth for the building, area of the building, content damage values and the building use are required to be validated.

Of the above, initially the survey building locations were manually cross linked with the building footprint GIS layer, as the GPS locations taken in the survey were inaccurate to correctly identify the surveyed building. For this purpose, the addresses and the appearances recorded in the survey were cross checked with the locations provided in the Google maps and imagery provided in the Google Street view, for all 417 survey locations. At the same time, the building use was confirmed with the imagery, which was correctly recorded in the survey, for more than 95% of the time.

At the identified buildings, the building floor area was cross checked with the recorded floor area from the survey, which did not match perfectly for each other. The reasons for this could be the roughness of the estimations, plus the errors in the size of the footprint layer. After identifying the buildings, the recorded inundation depth was cross checked with the inundation depth provided by FLO-2D model outputs for 2010, 2016, 2017 and local flooding. The results of the comparison are shown in Figure 10, in Annex 7.2.2.

4.2. Analysis of data

A total of 219 successive[1] buildings were filtered out for analysis, after the validation of the data points. Initially 10 main building subcategories are recognized by furthermore exploration, based on the based values as explained in section 3.2, into the survey details which are listed below.

- Groceries in residential buildings (Com/Res Grocery)
- Grocery

[1] *The term successive is used to indicate that the successive survey points matched with the building footprint layer (GIS format), and had the content damage values recorded. The total number of the survey points is 417, where some of the points were not found on the building footprint, where another set of locations failed to provide the content damage for the relevant flood locations.*

- Communications and bookshops
- Garages
- Spare parts centers and service centers
- Hardware stores
- Mechanical shops (iron-work/lathe/glass/welding and workshops)
- Medicine related (Pharmacies/dispensaries)
- Offices
- Restaurants/Tea shops
- Textile shops
- Miscellaneous (beer shops/salons/timber workshops)

The relationship between the damage values and the surveyed flood depths are shown in Annex 7.2.3. The base values for each damage category was derived based on the highest recorded damage per area value for a 3 m flood height, as listed in Table 2,

Table 2. Base values for the initially identified building use categories

Building Use	Base value used LKR/m^2
Garages	10703
Spare Parts and Service	1058
Com/Res Grocery	4890
Communication	9203
Grocery	6949
Hardware	34007
Mechanical	20586
Medicine	9004
Offices	72959
Restaurant	3530
Textile	25325
Misc.	6492

However, these building categories were recategorized in to three categories, based on the base values, as shown in Table 3. It should be noted that the revised base values for the new building clusters were derived considering the number of the buildings in each initially identified category and the derived base value for each initially identified building category.

Table 3. Reclassified building clusters

Cluster	Initial building category	Derived base value (LKR)	Number of buildings	Base value*Number of buildings	Weighted mean base value
Cluster 01	Hardware	34,007	20	680140	29121
	Mechanical	20,586	7	144102	≈ 29100
	Textile	35,325	10	253250	
Cluster 02	Garages	10703	16	171248	6180
	Spare Parts and Service	1058	10	10580	≈ 6200
	Commercial Residential Grocery	4890	59	288510	
	Communication	9203	11	101233	

	Grocery	6949	30	208470	
	Medicine	9004	7	63028	
	Restaurant	3530	9	31770	
	Misc.	6492	9	58428	
Cluster 03	Offices	72959	7	510713	72959 ≈ 73,000

4.3. Derivation of the damage indices and damage functions

The damage index was derived based upon the following equation, for each of the categories mentioned in the previous section, in the same manner explained in Section 3.2.

$$Damage\ Index = \frac{Recorded\ content\ damage\ value}{Weighted\ mean\ base\ value\ of\ the\ relevant\ category}$$

According to the definition above, three damage curves were derived for the three building use clusters.

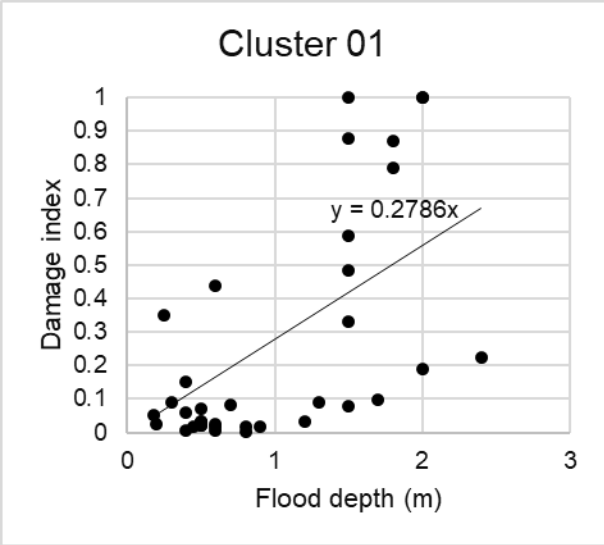

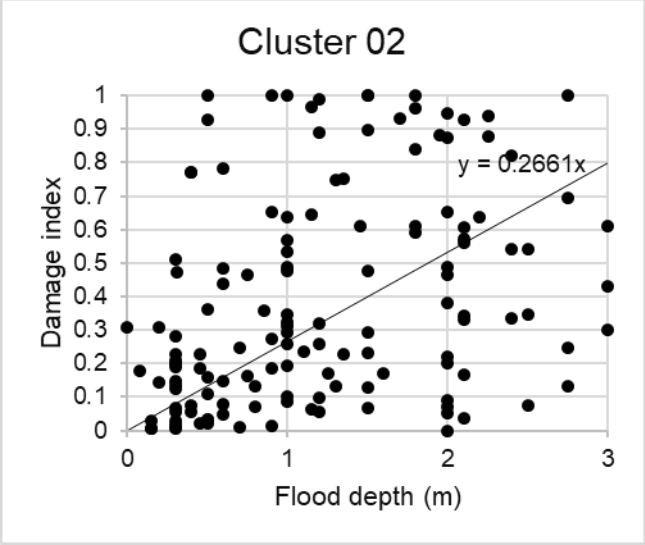

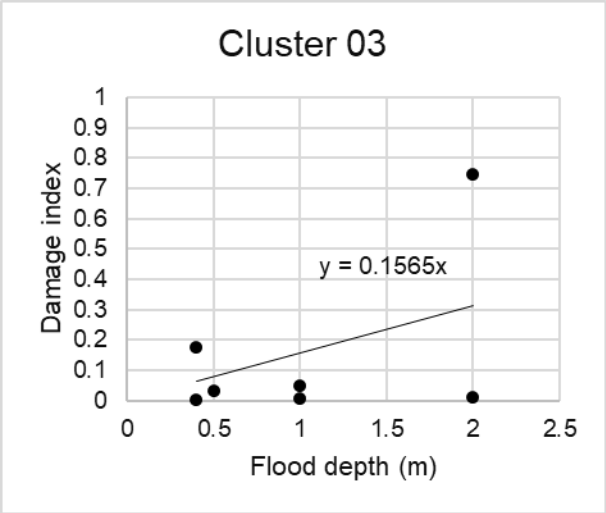

Figure 3.Flood damage curves for 1) Cluster 01 buildings, 2) Cluster 02 buildings 3) Cluster 03 buildings

The derived damage functions for the aforementioned building categories can be summarized as in below.

Table 4. Damage functions for content damage

Cluster	Building category	Base value (LKR/m^2)	Damage function where D = damage, x = water depth
Cluster 01	Health sector buildings	29,100	$D = 0.2786x$
	Industrial buildings		
	Warehouses		
Cluster 02	Educational	6200	$D = 0.2661x$
	Residential		
	Shops		
	Vacant buildings		
Cluster 03	Office buildings	73,000	$D = 0.1565x$

A sensitivity analysis was carried out to find out the sensitivity of the content damage, using the clustered approach and the building category wise (lump) approach to calculate the content damage, using a sequence of flood scenarios. The obtained damage values for each of the building categories and the flood scenarios can be found in Annex 0.

4.4. Short discussion

The modelled flood heights seem to appear after 0.5 m in most of the cases. This could be due to i) plinth height is not considered in the FLO-2D models, and ii) the inundation depths were recorded from the plinth level, in the survey. However, for the simulation purposes, the modelled flood heights will be used in the future, therefore it is important to have a moderating mechanism to convert the modelled flood heights to the actual flood heights.

The building footprint layer is having a limited number of building uses, compared to the breakdown of the building uses specified in this study. Therefore, for a particular building type, the damage should be considered proportionately, based on the number of the buildings from each sub category. From this, a generalized damage curve for aggregated buildings can be generated, which are weighted according to the number of buildings.

5. Damage assessment-implementation methodology

5.1. Damage calculation (vector format)

The damage calculations are done based on the vector formats, as the original exposure data is available in the building footprint layer, henceforth can produce accurate results. All of the vector calculations were performed in the ARCGIS platforms. However, the flood hazard maps (inundation maps) which are produced by the flood simulation software (FLO-2D and MIKE 11) produce raster files of the specified resolutions. Therefore, initially the flood depths at the building locations were extracted to the building footprint, using the building centroid location. Here the building layer was required to have separate

attributes to store the flood heights for different flood scenarios, as well as to store the base damage value for building type and the damage values.

Next, a custom-built model is run to calculate the damage values, for different damage types (structural and content). A snapshot of the model in the ArcMap platform is shown below (left: structural damage calculating model, right: content damage calculating model).

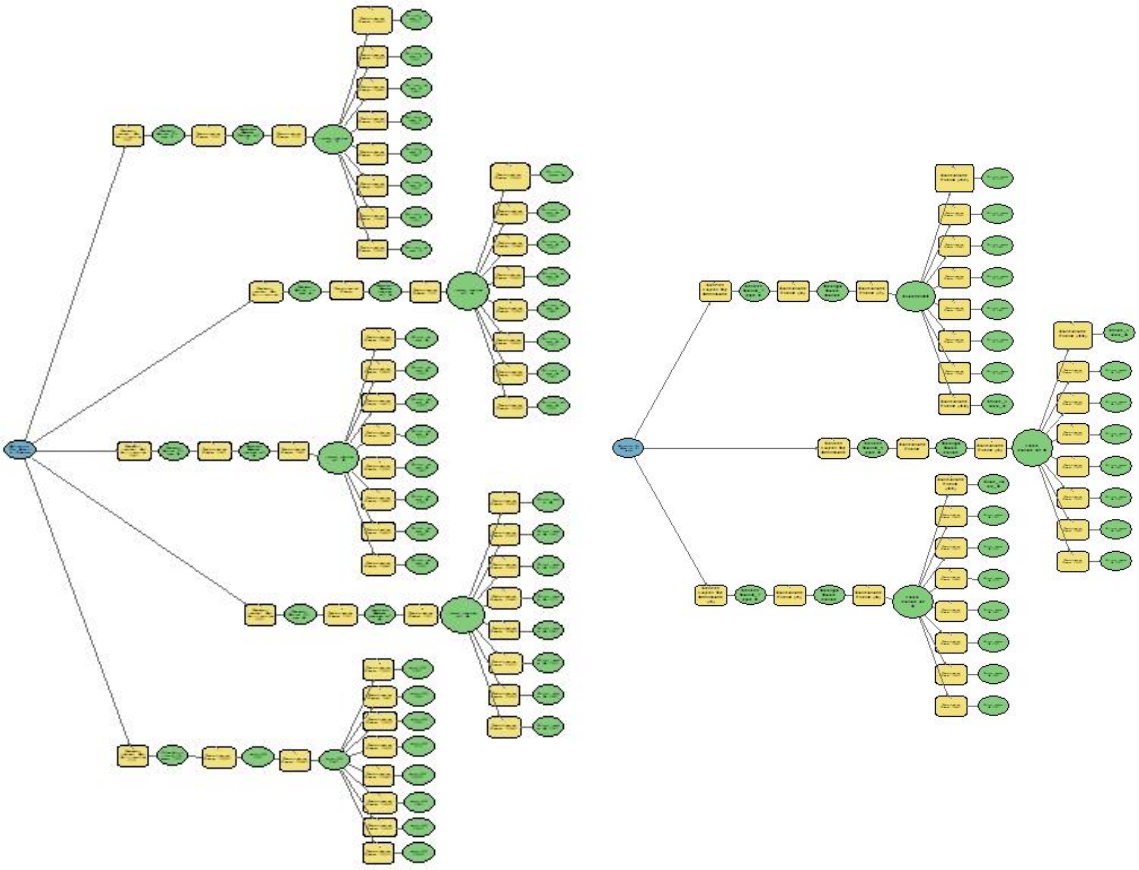

Figure 4. ARCMAP models for structural damage calculations (left) and content damage calculations (right)

The steps in the above models can be described as follows.

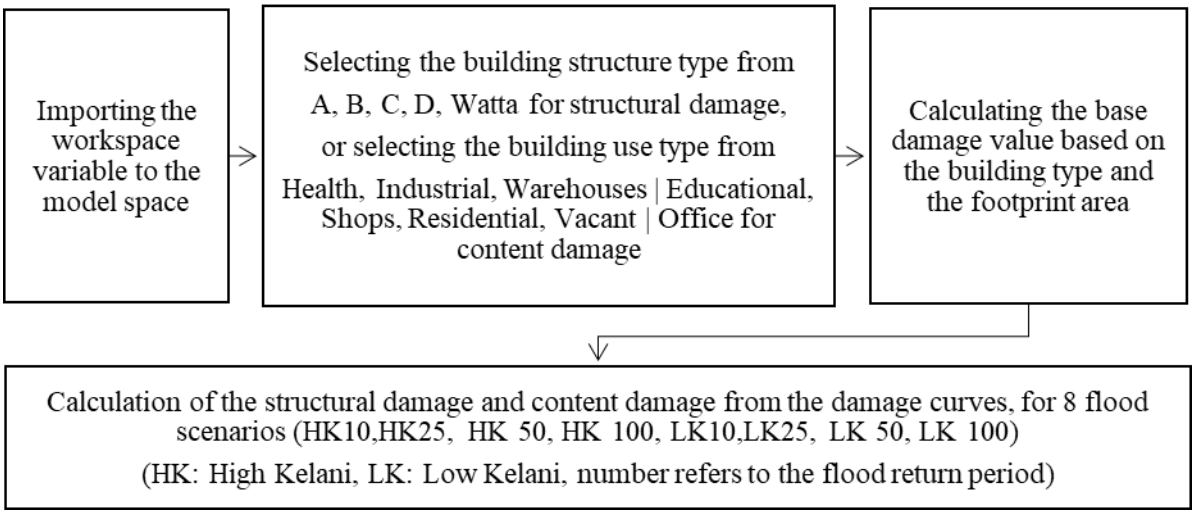

Figure 5. Methodology of the damage value calculations (vector format)

After running the modes for each type of damages, the results can be summarized according to the building structure type or to the building use type. Finally, the total damage can be taken, as well as the distribution of the damages can be taken. A produced result for the HK50 condition is shown below.

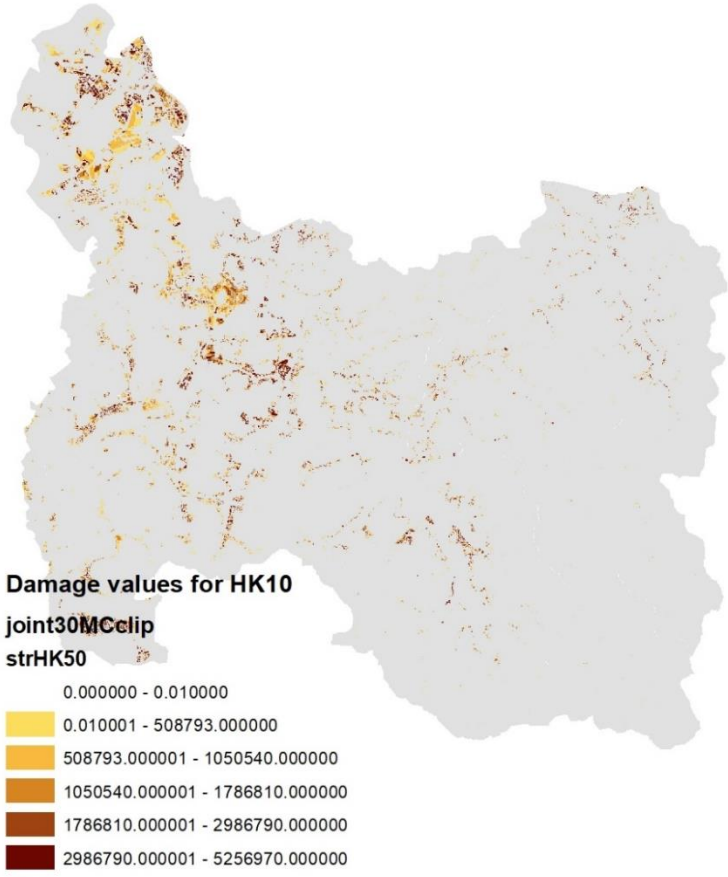

Figure 6. Damage values for a selected flood scenario

However, these vector format calculations consume a lot of computational time and effort, therefore it was decided to employ raster calculations for the damage assessment purposes. With raster format, these calculations could be performed within seconds using numerical calculation platforms such as Mathematica or MATLAB, and the requirement of manual labour is minimized, as these calculations can be automated.

5.2. Damage calculation (raster format)

For raster calculations, a similar method which was used in the section 5.1 will be used. The only difference is that for this purpose, the exposure information has to be prepared as raster (ASCII) files. Since the flood maps are already prepared in asci formats, the newly prepared building property raster files were prepared to match the properties of the flood extent layers. The highest resolution floods maps being prepared are having a grid size of 30 m, therefore the to-be prepared building property layers' resolutions was set to be 30 m. Additional properties of the raster files appears as follows.

ncols 492; nrows 533; xllcorner 396935.0; yllcorner 482565.0; NODATA_value -9999

Therefore, a grid of 30 m cell size was prepared and overlapped with the existing building layer, and the building properties were extracted to the grid, so for each building type, a cell in the grid would contain the percentage of each of the building type/use. Then for each type of building type and use, a raster file was generated. A comparison between the building properties in the vector format and the raster format is shown in Annex 7.4.

Now, the obtained raster files can be used to evaluate the structural and content damage values for different flood scenarios. First, the percentage values of the building property raster layers have to be converted into the area values, by multiplying all the cell values by 30 x 30 x 0.01 individually. Then these obtained values should be multiplied by the damage values matrix, which is obtained by subjecting the flood raster matrix elements in to the damage function and multiplying the answer by the base value of the respective building type/use.

5.3. Comparison of the results given by raster and vector methods

In order to adopt the raster approach of calculations instead of the vector calculations, the accuracy of the results from these two calculation methods should be assessed. For this purpose, independent damage evaluations were done using the vector method and the raster method for the flood scenarios which are having a resolution of 30 m. The selected flood cases are HK10, HK25, HK50, HK100, LK25, LK50, LK100 for existing conditions and with all of the flood mitigation interventions. The results of the raster and vector runs are shown below (from next page). For the calculations, please refer the Annex 7.5.

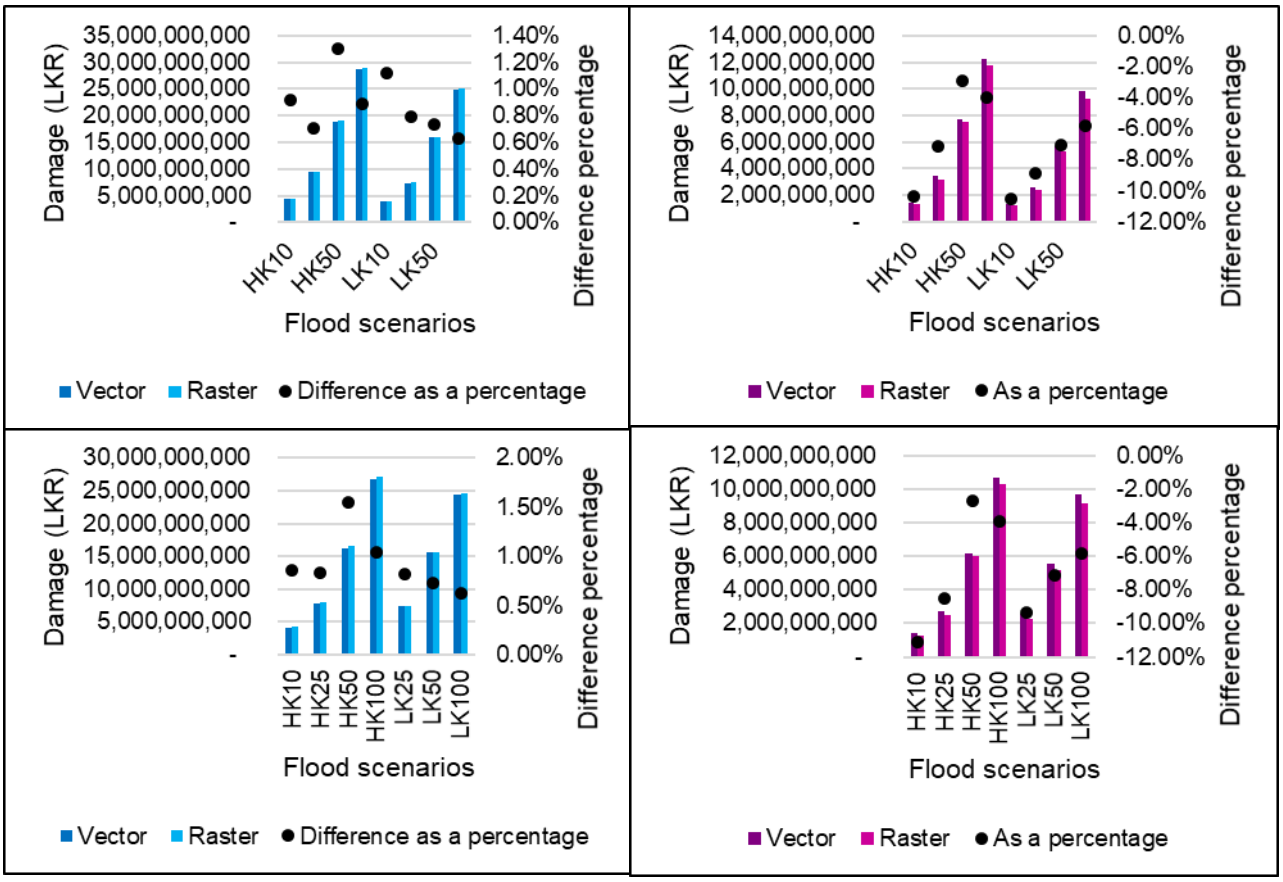

Figure 7. Comparison of vector and raster calculations Up Left: Structural damage for existing conditions, Up Right: Content damage for existing conditions, Down Left: Structural damage with all interventions, Down Right: Content damage with all interventions

Looking at the damage values obtained for structural and content loss, it can be seen that the variations in the estimations of the building structural damage are much less than that of the content damage. However, all of the damages fall below 10% of the vector processed value. Therefore, it can be concluded that it is okay to perform the damage calculations from raster formats, rather than converting them to the time and labour consuming vector computations.

5.4. Projecting for the content damage of the residential buildings

As aforementioned, the derivation of the content damage functions of this report is based on a field survey on the content damage of the commercial and industrial buildings of the flood affected areas, and the content damage of the residential units was not covered in this context. However, for the complete computation of the content damages, it is essential to establish a damage value for the content damage of the residential units. Therefore, three methodologies were used to estimate the content damage of the residential buildings, as shown below.

- Using the cluster 02 depth-damage function for the estimation of the residential content loss: this method is adopted as there were many commercial units which are established as a part of the residential unit, such as small retail shops. Cluster 2 depth damage curve estimates the content damage for the commercial units, and it also has the lowest base damage value. Therefore, it is

assumed that the content loss of the commercial units (cluster 2) will be equal to the content damage of the residential buildings.

- Using a portion of 25% of the structural damage which is occurred for the residential buildings: this method is recommended and used in the PHRD study for Metro Colombo floods.
- Using a conservative percentage of 60% of the structural damage caused to the buildings.

In order to identify the consistency of the results generated by above three approaches, the results generated from above three methods for different flood scenarios are compared, and the results are shown below.

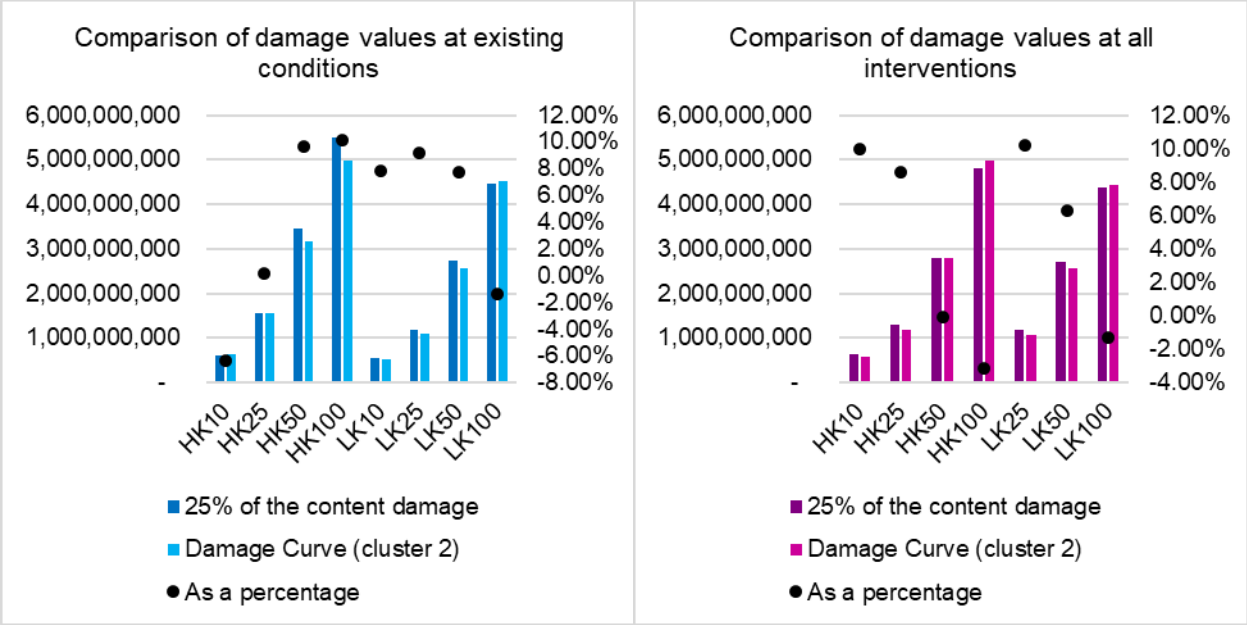

Figure 8. Comparison of the projected damage values for residential buildings. Left: Existing conditions, Right: All Interventions

From the results, it could be seen that the damage values obtained by the content damage functions and by the 25% of the structural value are very similar, therefore the cluster 2 damage functions could be used for the estimation of the content damages.

5.5. Conclusion

Using the damage curves developed under section 3 and 4, with the other workarounds as described by section 5, CUrW now possess the ability to rapidly calculate the economic loss from a flood event. The relevant damage curves are presented in Table 2 and Table 3.

6. Way forward: Identifying spatial distribution of the economic activities

In the damage assessment categories, another explorable category is to identify the loss of economic activities, due to the floods. This loss of economic activities is most likely to be generated from the business interruptions. Hence, if the business generation volume can be identified for a given geographical region, then that could be correlated to the gross domestic production of the particular

region. The business generation for a business is believed to be greatly expressed by the Value Added Tax (VAT) value and the Nation Building Tax (NBT) value.

With the use of the aforementioned spatial business generation, the business interruption due to a flood can be quantified in a meaningful manner. And it will start to capture the indirect tangible damages of the flood events. The calculation methodologies can be adopted as in section 3 and 4.

7. Annexes

7.1. Annex 01 - Source for structural damage curves

Development of generalized loss functions for rapid estimation of flood damages: a case study in Kelani River basin, Sri Lanka

Applied Geomatics
https://doi.org/10.1007/s12518-017-0200-4

ORIGINAL PAPER

Development of generalized loss functions for rapid estimation of flood damages: a case study in Kelani River basin, Sri Lanka

Akinola Adesuji Komolafe [1,2] · **Srikantha Herath** [1,3] · **Ram Avtar** [1,4]

Received: 9 September 2017 / Accepted: 10 November 2017

Abstract Assessment of infrastructural vulnerability to natural hazards, and subsequent economic loss, can make important contributions to future disaster risk minimization. The recent endeavor is to ascertain and evaluate risk globally, which can provide a framework to identify unique regional vulnerabilities, the mobilization of international investments, and cross-country risk comparison. This would require a concerted effort for the detailed classification of building exposures and vulnerability models. This study presents the design and efficacy of flood-vulnerability models for structural building types. The study uses an empirical approach, with data gathered from survey questionnaire, for direct estimation of flood damages in the Kelani River basin in Sri Lanka. Survey questionnaires were administered in the flood-prone areas of the basin, and depth-damage functions were established for four (4) structural building types that were identified based on the relationship between inundation depths and flood damage ratio. Event-based flood hazards were simulated using the Flo-2D model. Building exposures and densities were derived from remote sensing data, using integrated thematic land cover feature indices and supervised image classification. A modified mathematical loss model was employed to simulate flood damages to each building category for a disastrous flood event in the Kelani River basin. Simulated damages and post-flood survey showed reasonable comparativeness. The models can be employed for loss estimation of future damages and risk-reduction planning for flood disaster in Sri Lanka.

Keywords Loss functions · Exposure · Global risk assessment · Disaster risk reduction · Flood damage estimation · GIS · Flood hazards

Introduction

Flood-prone areas of the world are burdened with many risks resulting from increasing exposures and economic activities, and with climate change, there will be greater exposure to extreme weather events and an increase in flood impact (Giang et al. 2009). Preparedness for these events requires adequate estimation of potential risks for effective adaptation measures and mitigation. Traditionally, flood-risk analyses examine the characteristics of flood hazards and the gravity of different events, which are displayed on maps denoting potential risk. To enhance understanding of flood extent and depth analysis, various hydrological models have been developed to ensure accuracy and reduce large uncertainties of flood simulation outputs (Cammerer et al. 2013; Freni et al. 2010; Merz et al. 2010; Moel and Aerts 2011). Notwithstanding, potential consequences of flood hazards are not well determined, regarding specific vulnerabilities, which are often expressed in monetary terms (Cammerer et al. 2013). For this reason, many approaches have been developed to evaluate flood economic damages (Dutta and Herath 2001; Dutta et al. 2003; Herath et al. 1999).

Typical post-flood surveys are laborious and time consuming, giving rise to the flood damage modeling approach (Giang et al. 2009; Islam and Ado 2000; Merz et al. 2010). In recent years, flood damage modeling has witnessed growing attention as a prominent component of flood-risk analysis (Dutta and Herath 2001; Dutta et al. 2003; Heisten and Davdge 2005; Herath et al. 1999; Islam and Ado 2000; Merz et al. 2010). Although it is relatively new (Cammerer et al. 2013), it has become vital, given that most flood-risk

✉ Akinola Adesuji Komolafe
aakomolafe@futa.edu.ng

[1] Institute for the Advanced Study of Sustainability, United Nations University, 5 Chome-53-70 Jingumae, Shibuya, Tokyo 150-8925, Japan

[2] Department of Remote Sensing and Geoscience Information System (GIS), Federal University of Technology, P.M.B. 704, Akure, Ondo State, Nigeria

[3] Ministry of Megapolis and Western Development, Battaramulla 10120, Sri Lanka

[4] Graduate School of Environmental Science, Hokkaido University, Sapporo, Japan

Published online: 30 November 2017

reduction investments are based on cost benefits analysis (CBA). Calculation of flood economic damage is performed by scientific communities and policy makers for flood-risk prevention and reduction, assessment of flood vulnerability, flood-risk mapping, deliberation on flood mitigation measures, comparative risk analysis, and financial appraisals for re-insurance sector and financial appraisals during and immediate after floods (Cammerer and Thieken 2013; Cammerer et al. 2013; Dutta et al. 2003; Herath et al. 1999; James and Hall 1986; Merz et al. 2010). Rapid estimation of flood damages utilizes stage-damage curves from which mathematical functions are generated and integrated with flood hazard characteristics, exposures, and the value of elements at risk (Dutta et al. 2003; Herath et al. 1999; Herath and Wang 2009). These are then simulated using geographical information systems (GIS) to estimate both aftermath and potential damages of various flood scenarios. Stage-damage functions (known as vulnerability or loss functions) are an integral component of risk analysis, particularly for estimating economic losses from flood disasters. It establishes relationship between the rate of flood damage categories and flood characteristics, such as water depths, duration, velocity, and sediments. Several studies have been done considering flood water depths as the primary source of damages. Other flood characteristics, such as wind, velocity, and duration, have also been investigated (Herath and Wang 2009; Kelman and Spence 2004; Kreibich et al. 2005). Accuracy of the damage estimation has been investigated by different scholars (Freni et al. 2010; Jonkman et al. 2008; Komolafe et al. 2015; Notaro et al. 2014). Sources of these uncertainties have largely been attributed to the complex nature of flood-wave propagation processes (especially in urban watersheds), lack of data for validation and calibration, insufficient damage modeling approaches, landuse data, and incomplete flood damage classification.

Flood damage classification is a major contribution to damage estimation. Flood damage categories are classified as tangible and intangible. Tangibles are further classified as direct and indirect. Direct damages are caused by concrete contact with flood water, such as loss of life. Indirect damages are abstract impacts, such as emotional trauma or loss of productivity and income (Jongman et al. 2012). Damage and loss estimations have been derived for various categories of tangible properties, such as residential, commercial, and agricultural crops (Dutta and Herath 2001; Dutta et al. 2003; Herath et al. 1999; Kreibich et al. 2005). Most of these categories are aggregated and do not reflect detailed components of different structural responses to flood water. More detailed unified loss functions, that are applicable globally, are required to enable the comparison of losses between countries, which would lend access to common adaptation and mitigation sources. Also, subdividing building exposures to ultra-specific categories, according to de Moel et al. (2012), would allow for more detailed stage-damage functions and improved differentiation of economic values at risk. The objective of this study is to present and validate vulnerability functions for global building types in the Kelani River basin, Colombo, for urban river flood disaster risk management, as classified by the United Nations office of Disaster Risk Reduction (UNISDR) in Kelani basin, Colombo, Sri Lanka.

A number of studies have been carried out on flood damage assessment in Sri Lanka, despite incessant occurrences of floods caused by excessive rains. Most of these studies are based on post-flood surveys by the Ministry of Disaster Management and World Bank (DMC 2010). Other scholars have attempted to develop loss functions for the estimation of flood damages in Sri Lanka concentrating primarily on the impact of the 2004 Indian Ocean Tsunami flood (Kimura et al. 2006; Murao and Nakazato 2010; Peris 2006). Sri Lanka was one of the most affected countries by the Indian Ocean Tsunami in 2004, with about 40,000 human casualties and 96,000 homes destroyed (Murao and Nakazato 2010). A tsunami is a series of long massive waves generated by an undersea disturbance caused by earthquake or volcanic eruption under the Ocean. These immense waves devastate most coastal dwelling places due to gross elevated flood rising. Stage-damage curves, in response to tsunami floods, were generated from field surveys (Kimura et al. 2006; Murao and Nakazato 2010) and data captured by the Department of Census and Statistics of Sri Lanka (Peris 2006). Fragility curves were constructed taking into account the relationships between building damages and tsunami heights of major coastal cities in Sri Lanka. Implementing established functions, such as fragility curves, has good merit for urban safety planning for catastrophic or natural disasters. However, such functions may not be applicable when preparing for damages caused by urban flooding, arising from excessive rainfalls or river overflow. Urban river flooding from gross rainfall is a recurring event in Sri Lanka and should be afforded priority in future disaster risk-reduction planning. Sri Lanka often experiences flooding and other climatic-related disasters. Flood events, which occur almost every year during monsoon seasons (April to June and September to November), are threats to most of the river basins in the country, especially the study area (Kelani), Kalu, and Gin River basins (Niroshinie et al. 2011).

The study area

The Kelani River basin is one of the most vulnerable basins in Sri Lanka. It stretches to approximately 192 km long with a catchment area of about 2,292km^2. It is the fourth longest river in Sri Lanka. The river flow, which mostly depends on the season, and the three operational reservoirs, is an average of 25m^3/s in dry periods and ranges between 800 and 1500 m^3/s during rainy seasons (Ministry of Irrigation Resources, S. L. 2009). The catchment is naturally divided into two: the steep

and flat terrain (based on the topography), comprised of the upper and the lower catchment, respectively (Fig. 1). The lower catchment is a plain area that receives much water from the upper basin, which often results in overflow. Compounded with poor drainage systems, there is continuous flooding in this area. The average annual rainfall is estimated to be about 3450 mm and a total rainfall of about 6000 mm yearly. The lower part of the basin (about 500km^2) lies within most parts of the Colombo District, which is the most densely populated area and is the hub of commercial activities of Sri Lanka. Because of the high flood risk it poses to Colombo, the commercial capital city (largest city in the country), a comprehensive flood-risk evaluation, encompassing flood forecasting to flood-risk modeling, is very essential to assuage or circumvent disaster risk in this region, as well as the entire country. Historically, most devastating flood events, which resulted in ruin to both public and private properties, were recorded in years 1989, 1992, 2005, 2008, and 2010 (DMC 2010; Niroshine 2012). The basin is projected to experience a series of disastrous flood events as a consequence of climate change, which will inevitably result in tremendous losses, especially in Colombo City. Estimating potential damages that could occur from various weather events is greatly essential to effectively plan for disaster risk reduction and risk management. This can be achieved by utilizing loss functions for efficient estimation of expected damages.

Methodology

To meet this study's objective—to establish and validate loss functions for global building types—event-based inundation extents and depths were simulated using hydrodynamic models to enable detailed survey in the flood-affected areas within the basin. Stage-damage function curves were developed from the acquired empirical damage data. The exposures were mapped with the aid of remote sensing data. The flood hazards, stage-damage functions, exposures, and values of element at risk were integrated in GIS to estimate the flood damages for each building structure for the simulated historical flood event. The results of the total damages were compared with the observed damage data to validate the loss models.

Flood inundation modeling

An event-based approach was applied for comparison and validation of the output from the flood model and economic risks. Data can be readily gleaned from flood hazards, on the extent and intensity. Identification and mapping of flood hazards, for a specific event, are important aspects of flood-risk assessment. Although multiple flood characteristics (e.g., water depths, duration, sediment, wind, and velocity) are responsible for damages in any flood event, water depth is considered in this study as a major damage factor to urban building structures. Flood simulation was performed (for May 2010 flood events in Kelani River basin) using SHER model (Herath et al. 1992; Herath et al. 1990) within the NK_GIAS GIS framework and Flo-2D model. The basin was divided into two: lower Kelani (downstream) and upper Kelani (upstream). The upstream, with high elevation, receives much rainwater and subsequently discharges into the downstream (made mostly of residential and commercial areas), which often resulted into floods. The flow that discharges from upstream was simulated using the SHER model. The inundation modeling was done using Flo-2D with the outflow of the upstream, as the inflow to the downstream. Flo-2D is an integrated GIS and hydrological model (by Flo-2D Software, INC, Arizona, USA). It is a volume conservation flood-routing model that can be used to simulate overland and channel flow over a complex topography. It is also a physical process model that routes rainfall-runoff and flood hydrographs over unconfined flow surfaces or in channels using the dynamic wave approximation to the momentum equation (Flo-2D 2009). Its two-dimensional flood-routing capabilities are accomplished by numerically integrating the equation of motion and conservation of volume for flood water. The distribution of flood waves within the flow domain is controlled by topography and resistance to flow (Flo-2D 2009). The software is a grid-based system that makes use of the interface, Grid Developer System (GDS), with the ability to simulate floods, using various grid attributes, such as rainfall and infiltration, hydraulic structures, channels, levees, n values, and evaporation (Flo-2D 2009).

Governing equations

The Flo-2D model is made up of general fluid equations: the continuity and dynamic wave momentum (motion equation), as displayed in Eqs. 1 and 2.

$$\frac{\partial h}{\partial t}+\frac{\partial hV}{\partial x}=i \tag{1}$$

$$S_f=S_o-\frac{\partial h}{\partial x}-\frac{V}{g}\frac{\partial V}{\partial x}-\frac{1}{g}\frac{\partial V}{\partial t} \tag{2}$$

where h is the flow depth and V is the depth-average velocity in one of the eight flow directions x. I, S_f, and S_o denote the excessive rainfall intensity and friction slope, which is determined by the manning equation and the bed slope pressure gradient, respectively. The equation actually represents one-dimensional depth-average flow; however, because the Flo-2D is a multi-directional flow model (eight potential flow directions), the equations are applied over grid elements, by computing average velocity flow in one direction at a time (Flo-2D 2009). The eight flow directions are the following: the four cardinal directions (north, south, east, and west) and

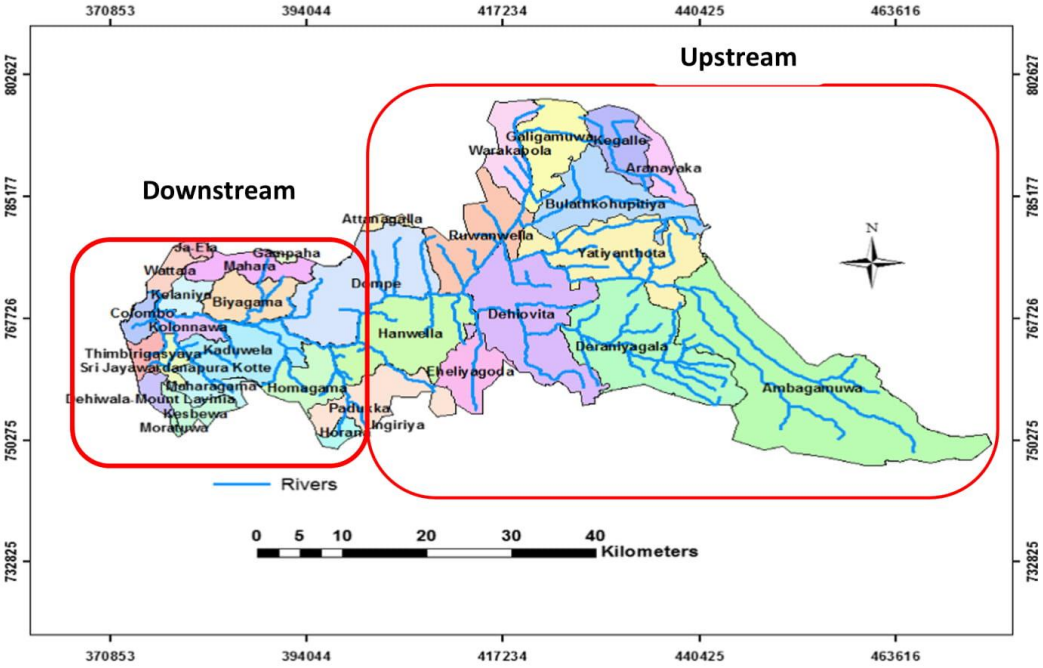

Fig. 1 Study area: Kelani River basin

the four diagonal directions (northeast, northwest, southeast, and southwest). The system computes each velocity of flow independently of the other seven directions, in one dimension, with the stability controlled by the magnitude of the variable computational timesteps (Ahmed and Gerlach 2012; Flo-2D 2009). It calculates the net change in volume as the product of the net change in discharge and timestep; the change in depth is determined by the net change in volume with the surface area of the cell (Ahmed and Gerlach 2012). The model consists of fifteen components: reduction factors, streets, infiltration, inflow and outflow elements, rain, floodplain cross-sections, levees, hydraulic structures, multiple channels, breach, mudflo-2D, mudflow and sediment transport, and evaporation.

Grid development and model inputs

Approximately 2,292km^2 of the basin was divided into two: upper and lower. The upper acts as the inflow source to the lower basin, which causes frequent heavy flooding in the mostly urban and commercially situated areas. The grid was created using elevation data. The topography data were obtained from the Department of Survey, Colombo, from which the digital elevation model (DEM) was developed. The grid cell size of 250 m was assigned to enable fast simulation of the flood events. The roughness coefficients were assigned based on the Chow (1959) rain-runoff model (Table 1) using the landuse map of the study area. Manning coefficients were assigned to the shape file in ArcGIS and exported to the Flo-2D grid where they were computed and distributed within the grid. The Green Amp method of infiltration was used for the simulation. The Green Amp method utilizes initial loss, initial saturation, capillary suction head, hydraulic conductivity, and soil porosity. These components were assigned based on the soil types of the study areas. For the lower Kelani basin, the majority of the soil types (about 70%) are loam. Based on existing literature (De Silva et al. 2012), the capillary suction head, hydraulic conductivity, and soil porosity of loam is 90 mm, 13.2 mm/s, and 0.463, respectively. These were assigned and distributed within the grid.

Hydrology

The discharge, which was used as inflow to the lower Kelani, was derived from the upper Kelani basin. This was simulated using similar hydrologic element response (SHER) model. The modeling system is made up of the submodels of surface, subsurface, and aquifer. The surface model uses kinematic wave equation for surface flow computations, while the subsurface model uses the one-dimensional Richard's equation. For the aquifer model, Darcy's flow is assumed (Herath et al. 1992; Herath et al. 1990; Herath et al. 1995). The modeling

Table 1 Manning's n values assigned to rain-off model (after Chow [1959])

Land cover	Manning coefficient
Urban	0.0.15
Forest	0.035
Crops	0.035
River	0.010
Road	0.016
Crop/grass	0.035

system can be divided into two types of blocks that represent similar hydrologic characteristics, such as recharging and discharging areas. Other sub-block areas, such as impervious, paddy, compressed soil, and compressed soil, can be assigned (Herath et al. 1992). In this study, watershed was divided into two: impervious and pervious blocks. The impervious comprises the roofs, roads paved, and all impermeable materials; the pervious blocks are the paddy fields, croplands, forest, etc.

Governing equations

i.) Impervious Model: this model uses the following equation:

$$\frac{dS_{imp}}{dt} = P - D_{imp} - E_{imp} \tag{3}$$

where P is the rainfall, S_{imp} is the water depth in the depression storage pond, D_{imp} is the surface runoff from the impervious model, and E_{imp} is the evaporation from the depression storage pond. This model makes use of the spill-over from the depression storage pond, as the surface runoff, while the evaporation value is considered small and assumed zero.

ii.) Pervious Model: this model uses three (3) water storage depths, which are computed by the following equations:

$$\frac{dS_1}{dt} = U_s - E_1 - D_s \tag{4}$$

$$\frac{dS_2}{dt} = P - E_2 - R - I - U_s + P_{al} \tag{5}$$

$$\frac{dS_g}{dt} = R - D_g - P_{a2} \tag{6}$$

where S_1 is water storage in the depression pond, S_2 is water storage in the subsurface layer, S_g is the water storage in the aquifer, D_s is the surface runoff, and E_1 and E_2 are the evaporation from the depression pond and subsurface layer, respectively; P is the infiltration to the subsurface layer (rainfall origin), R is the recharge to the aquifer, I is the interflows, U_s is the return flow, D_g is groundwater discharge to rivers, P_{a1} is the infiltration to the subsurface layer (irrigation water), and P_{a2} is the water pumped out from a well (Herath et al. 1995).

Data used for the simulation of the hydrology of the runoff at the Hanwella gauge station are the following: (i) rainfall data, (ii) soil parameters (such as saturated hydraulic conductivity [vertical], K0_v, saturated hydraulic conductivity [slope], saturated moisture content, Theta_O, saturated moisture content, Theta_R, Alpha, and Beta),(iii) manning coefficients, and (iv) aquifer parameters. The Kelani River basin was divided in the recharge and discharging blocks as shown in Fig. 2. After the hydrological simulation, the discharges at Hanwella, which is at the start of the flow to the lower basin, were extracted for the flood events (in 2010) and validated with the observed discharges for the same period. Model calibration was done by manipulating the simulation parameters to fit the observed data.

Apart from the failing limb, the peak and the rising limb of the simulated in-flow hydrograph (at Hanwella station) agree well with the observed discharge for the simulated flood event (Fig. 3). The efficiency of the model was assessed using Nash-Sutcliffe model efficiency coefficient (Nash and Sutcliffe 1970), which is defined as:

$$E = 1 - \frac{\sum_{t=1}^{T}\left(Q_o^t - Q_m^t\right)^2}{\sum_{t=1}^{T}\left(Q_o^t - \bar{Q_o}\right)^2} \tag{7}$$

where $\bar{Q}_{\text{o}}$ is the mean observed discharges, Q_{m} is the modeled discharge, and Q_{o}^{t} is the observed discharge at time t. The accuracy of any simulated model, using the Nash-Sutcliffe model, is determined by its closeness to the model efficiency of 1. The efficiency of the simulated model was calculated to be 0.98. This is deemed accurate as it is very close to 1.The output of the calibrated flood hydrograph (Fig. 3) served as the input to flood inundation modeling in Flo-2D, using the control parameters stated in Section 3.1.2.

Channel

Flo-2D's channel flow is simulated in the downstream direction in one dimension. This can be accomplished via trapezoidal, rectangular, or by using surveyed cross-sections, and is routed with the dynamic wave approximation to the momentum equation (Flo-2D 2009).

The channels and their geometry (cross-sections, roughness, channel widths, length of channel, bank

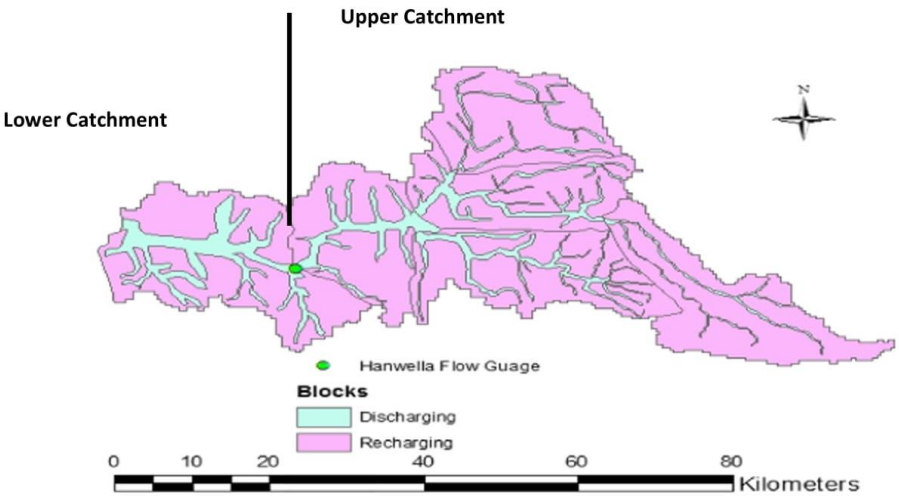

Fig. 2 The recharge and discharge blocks within the upper and lower catchments of the study area

elevations) are represented in the CHAN.DAT file. Only the Kelani Main River, from Hanwella to Nagalagam Street, was considered in the simulation. Channel was delineated in the Flo-2D grid, considering the flow direction from upstream to downstream, and river channel geometry was assigned based on the existing river cross-sections. River cross-sections from Hanwella, Atigala, Kaduwela, Ambatale, Kelanimulla, Wennawatta, and Nagalagam Street were incorporated to simulate the river flow with the floodplain grid elements flow. Hydrograph generated from the upstream at Hanwella served as channel inflow.

Flood simulation

Flood simulation was done in the floodplain mode using various control parameters. In order to ensure numerical stability (a very significant element in flood modeling), stability criteria and floodplain depth tolerance were selected. This was done in the Flo-2D simulation control interface. The default values for the floodplain and channel depth tolerance (DEPTOL), surface detention tolerance (TOL), and the maximum value for the numerical stability coefficient, for dynamic wave routing (WAVEMAX), are 0.2, 0.1, and 1.0, respectively. The model was initially simulated with the default stability parameters by a change to the surface detention tolerance (as 0.015) to improve the stability of the model. Simulation time set for the model was 264 h, accounting for the flood-event period being modeled (May 2010) while the out timestep is 1 h. The simulated inundation model was processed in the Flo-2D Mapper. With this interface, maximum flow depths and the floodplain final

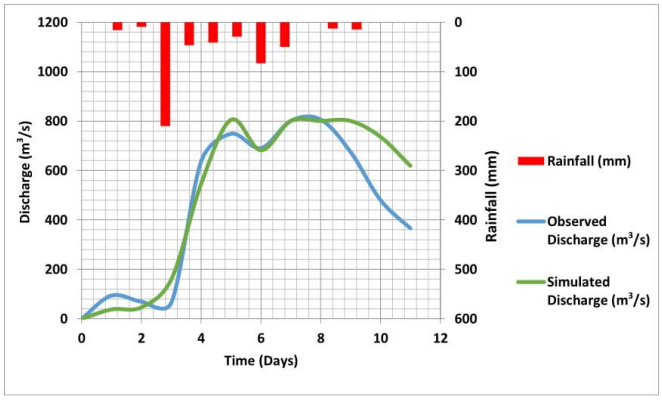

Fig. 3 Simulated vs. observed discharge and the rainfall for the May 14 to May 25, 2010, flood events at Hanwella station

Table 2 Global building types

No.	Category	Descriptions	Identified buildings in the basin
1	Wood	Wood	√
2	All steel structures	Steel light frame	–
3	All concrete frames	Concrete frame with unreinforced masonry infill walls	√
4		Reinforced concrete moment frame	–
5		Reinforced concrete frames and concrete shear	–
6	All masonry	Unreinforced masonry bearing walls	√
7		Reinforced masonry bearing walls	–
8	Adobe	Adobe	–
9	Slab	Flat slab structure	–

flow, as a function of depths, were created from the difference between maximum surface water elevation and the ground surface elevation of the study area. The outputs coded in shape files were exported into ArcGIS for further processing and analysis.

Development of loss functions curves

Building classification

In this study, the initial classification of exposure was based on the global building structural types classifications by the World Agency of Planetary Monitoring and Earthquake Risk Reduction (WAPMERR) as documented by the United Nations office of Disaster Risk Reduction (UNISDR), during a workshop on global risk assessment (Global Assessment of Risk) (Masqsood et al. 2013). (Table 2). UNISDR developed biennial global assessment reports on Disaster Risk Reduction (DRR). These reports contain comprehensive review and analysis of natural hazards and their overall effect on humanity.

At a 2013 GAR workshop, initial benchmark curves for the residential building categories were developed based on expert judgments, which was due to limited existing empirical vulnerability data in different countries.

Field survey and data processing

The survey questionnaire approach was applied in this study to obtain flood damage data for the establishment of loss functions for global residential building types. The field survey was carried out within the flood-prone area in the study basin, aided by the simulated flood map of the area (Fig. 4). A total of 297 flood damage data were collected in the study area on the economic loss impacts on the most recent floods. Respondents are mainly the adult family members with clear remembrance of the recent flood events in the study area. The data include the following: different building classes, repair, and replacement costs of the building structures, with their corresponding flood water heights, water duration, and building floor areas. Other parameters recorded in the field, such as content damages and non-economic impacts, are not included in this study. These data were collected with their corresponding global buildings types identified in the field. The acquired data were processed and analyzed statistically to derive loss functions, which establishes the relationship between structural damage extent and water depths.

Three (3) types of global residential building structures and commercial buildings identified in the field (and corresponding percentage distributions): (i) unreinforced masonry bearing walls (43%), (ii) concrete frame with unreinforced masonry infill walls (41%), (iii) wooden (9%), and (iv) commercial (7%) (see Table 2 and Fig. 5). These structures were recorded with their corresponding flood water depths and damage variables. Damage to structures was calculated based on damage ratio, which is the ratio of the repair cost of the structure after the flood event to the replacement (actual) cost of the structure, as expressed in Eq. 8.

$$Structural\ \ Damage\ \ ratio\ \ (\%) = \frac{Repair\ \ Cost}{Replacement\ \ Cost}^{*} 100 \tag{8}$$

For each category, data were plotted and correlated to derive the best prediction using structural damage as the dependent variable and water depth as the independent variable (the predictor). The models were predicted with logarithm functions expressed in Eq. 9.

$$D_f = C1 \times ln\,(x) + C \tag{9}$$

where D_f is the damage function, x is the flood water depth (m), and C and C1 are the damage coefficients at any given landuse type (Fig. 12 and Table 6).

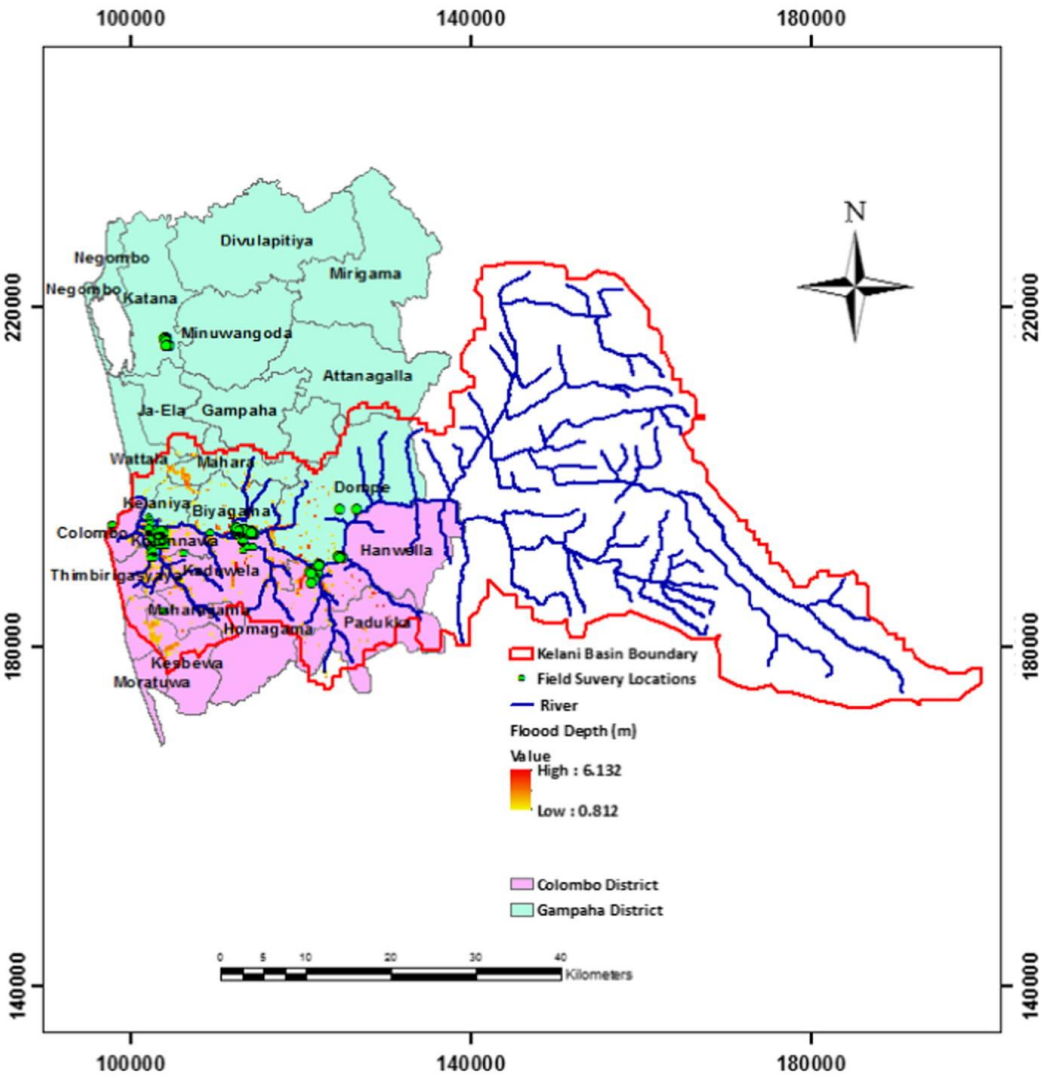

Fig. 4 Field survey locations

Exposures mapping

Built-up extraction from remote sensing data

Building inventory analysis is fundamental in flood disaster risk reduction, planning, and modeling. Flood-risk models require knowledge of the number of buildings within the squared grid for adequate damage or loss estimation (Dutta and Kamrujjaman Serker 2005). In order to carry out the grid-based damage simulation, the distribution of the properties exposed to the flood water depths would be essential. Remote sensing has proven to be an invaluable tool for mapping urban built-up areas (Ahmad et al. 2016; Bhatti and Tripathi 2014; Dutta and Kamrujjaman Serker 2005; Xu 2007). It is a unique technology that provides a synoptic view of the urban area, both in space and time, especially in an inaccessible area where ground survey cannot be carried out (Avtar et al. 2013; Maktav et al. 2005; Richards 2013).

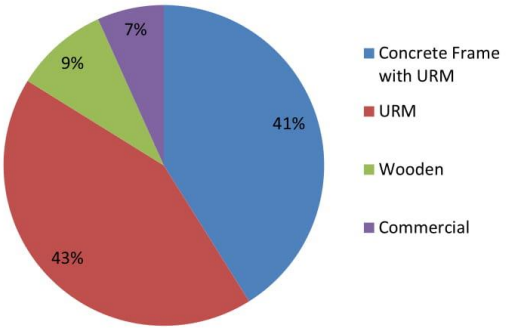

Fig. 5 Surveyed building types and their percentage distributions

Remote sensing data were used to extract the exposure information. Due to limited access to higher resolution data and the cloud cover in the study area, detailed exposure (building) mapping could not be carried out. However, Landsat 8 OLI imagery of the Kelani River basin area (path: 141, row: 55) acquired on April 14, 2015, obtainable from the United States Geological Survey (USGS), was used to extract the built-up areas within the basin. The image (in GeoTiff format), which covers the study area, with less cloud cover (5.07%), consists of eleven (11) spectral bands. Band 1 (coastal aerosol, 0.43–0.45 μm) and band 9 (cirrus, 1.36–1.38 μm) were excluded from further processing because they are not instrumental for the analysis. Landsat 8 OLI optical bands (2–7) are made up of 30-m spatial resolution; thermal bands (10 and 11) was 100 m, but had been resampled to 30 m by the vendors, Earth Resources Observation and Science (EROS) Center, United States Geological Survey (USGS); and band 8 is the panchromatic with a spatial resolution of 15 m. Projection used in this study is Universal Transverse Mercator (UTM) with zone 44 N and WGS datum. The image file extension was image file format (TIFF) and integer, with each band separately downloaded. All the bands (2–8 and 10–11) were layer stacked and clipped to the study area. Areas covered by cloud, within the study area, were considered negligible, and as such no atmospheric corrections were performed. Urban land use is made up of three principal components: the impervious surface materials (built-up), vegetation, and open water. Due to a mixed spectral, as a result of the urban land class heterogeneities, an integrated built-up extraction was applied, using the method developed by Xu (2007). The method incorporated the combination of three (3) thematic-oriented indices that represent three (3) urban land use components: (i) normalized difference built-up index (NDBI), (ii) soil-adjusted vegetation index (SAVI), and (iii) modified normalized difference water index (MNDWI). These components were integrated to effectively differentiate the built-up area from other urban landuse classes in the study area. NDBI was used to generate built area, SAVI was carried out to enhance the vegetation areas, and the MNDWI was analyzed to enhance the water bodies in the study area. All of the thematic images were integrated using principal component analysis (PCA) and threshold technique.

Table 3 Correlation values of the new composite thematic image with NDBI, SAVI, and MNDWI bands

	NDBI	MNDWI	SAVI
NDBI	1	−0.31156	−0.82965
MNDWI	−0.311555	1	−0.25298
SAVI	−0.829645	−0.25298	1

Built-up land extraction

Extraction of built-up land was conducted by integrating the three extracted indices. After the generation of these images (NDBI, SAVI, and MNDWI), a new image was formed by layer stacking the three indices into a single image. The new image reflects the three land cover features in three RGB colors (red: NDBI, green: SAVI, and blue: MNDWI). Correlations between these thematic bands are largely reduced (with the negative correlation as shown in Table 3), consequently with clear distinction among the three major landuse classes: vegetation, water, and built-up land.

PCA was implemented for the extraction of built-up land use from the new layer-stacked thematic image. PCA is a method of identifying patterns in data by highlighting their similarities and differences. It is a process of transforming a set of correlated variables into new uncorrelated variables. Due to its orthogonal transformation, which results in the uncorrelated new images, it is capable of differentiation among the three major landuse classes from the derived thematic image. It examines the principal components (Eigen vectors) to determine which of the image components will relate directly to the spectral signatures of specific target materials (Xu 2007). PCA was performed using forward principal component (PC) rotation to generate three PC images. The RGB color composite of the three PC images clearly differentiate the three landuse classes (Fig. 6). Table 4 shows the Eigen vectors of the transformed images, which are based on the covariant matrix, and determine which of the landuse classes (bands) has the highest influence in the image. In Table 4, PC1 enhances water (positive values) while suppressing the built-up and vegetation (negative values), which cannot be used for the extraction of built-up landuse. PC3 enhances both built-up and water body while suppressing the vegetation; in this case, built-up and water will be mixed up. Only PC2 yields a unique distinction between built-up land (positive values) and the other two classes (negative values). This was utilized for the extraction of built-up land.

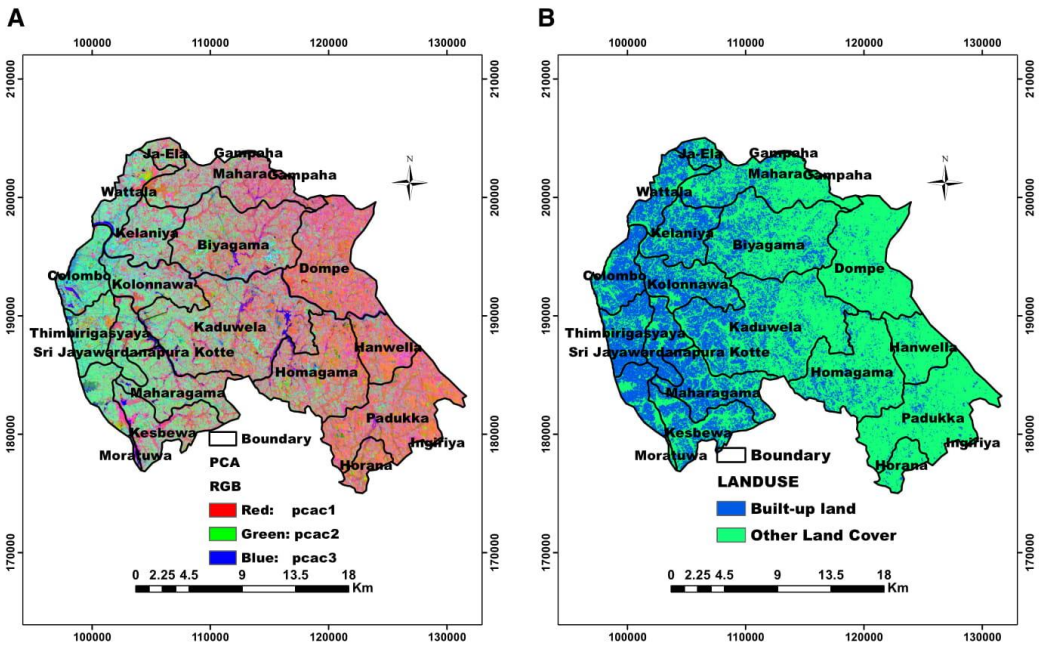

Fig. 6 **a** RGB composite of the PC1, PC2, and PC3. **b** Extracted built-up land

Finally, using threshold value (0.063) based on the Eigen vector of the built-up land, the PC2 image was classified into two: built-up land (values ≥ 0.063) and other land use (< 0.063), as shown in Fig. 6, and these were assigned 1 and 0, respectively. Accuracy of the derived built-up map was examined using confusion matrix. The image was compared with the ground truth data obtained from high-resolution Google earth image, with about 86% accuracy.

Building density estimation

Building density (BD) is defined as the number of building units in any given occupied area. It provides a quantitative measurement of the number of buildings expected within a unit area. In urban planning and development, BD is used as a tool for effective landuse planning, population distribution, and provision of public infrastructures. Landsat8 remote sensing data, as described above, was used to map urban densities in the study area. The Landsat image was classified into five areas: high dense urban, medium dense urban, low dense urban, water bodies, and vegetation as shown in Fig. 7. The high dense urban is mostly concentrated in Colombo, Sri Jayewardenepura Kotte, and Thimbirigasyaya divisional secretariats. Areas covered by water bodies and vegetation were not included in the density estimation. Only the area of urban classes (high dense, medium dense, and low dense) and the total number of buildings in 18 divisional secretariats (obtained from the Department of Census and Statistics, Sri Lanka) were combined in multiple linear equations (Eq. 10, Table 5) to derive the BD for the three urban classes.

Table 4 Principal components analysis (PCA) of the thematic bands

Eigen vectors	Bands	PC1	PC2	PC3
	NDBI	−0.7439	0.0633	0.6653
	MNDWI	0.2518	−0.8956	0.3667
	SAVI	−0.6191	−0.4403	−0.6503

$$B_i = \beta_i x + \omega_i Z + \delta_i Z, For = 1, 2, 3, 4, 5 \ldots . \text{n} \quad (10)$$

$B_i$is the total number of buildings (residential and commercial); β_i, ω_i, and δ_i are areas (km^2) covered by high dense urban, medium dense urban, and low dense urban, respectively; $x, y, and\ z$ are the BD (number of buildings per km^2) for high dense urban, medium dense urban, and low dense urban, respectively (Fig. 8)

We estimated the BDs for the high, medium, and low urban to be 4254, 1450, and 1162 buildings per square kilometer, respectively. These were further validated by multiplying each estimated BD by the land cover area for the density classes in each secretariat and compared with the measured number of buildings. Both the observed and estimated total number of

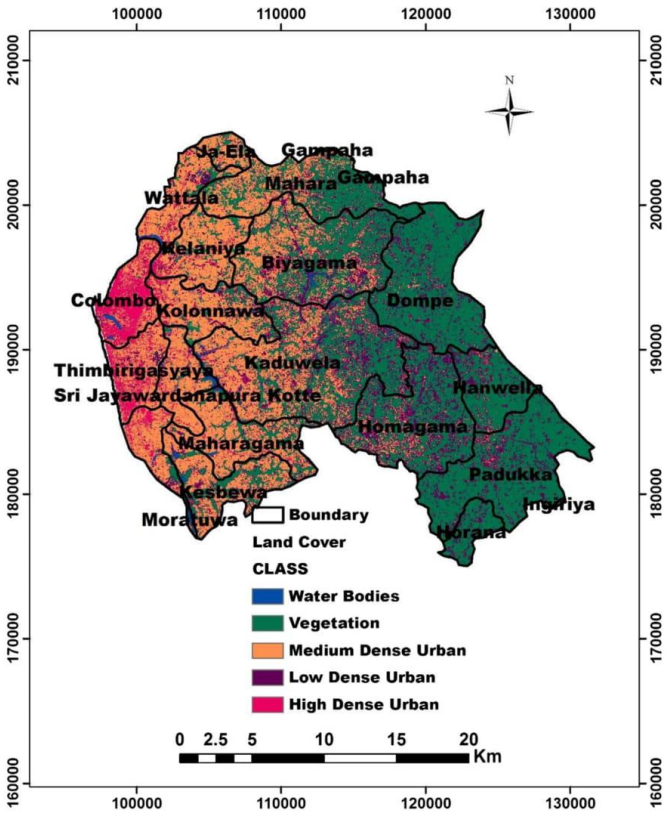

Fig. 7 Landuse classes derived from image classification

buildings showed good agreement (Fig. 9). The BDs were spatially distributed within the grid for flood damage estimation.

GIS-based flood damage modeling

Detailed loss functions established in this study were applied to the Kelani River basin and validated by the observed damage obtained after the flood disasters in May 2010. Lower Kelani River basin, which is the urban area mostly affected by flood, was considered for the application of the loss models developed in this study. The basin is comprised of two main districts: Colombo and Gampaha. Colombo District, which is host to the commercial capital city, Colombo, is the most densely populated district and also the most urbanized in the river basin. The total population of all the twenty sub-districts within the basin, according the Population Census (2012), is estimated to be 3,291,600. A GIS Grid-Based modeling was employed to simulate the total damages using the established loss functions (Fig. 10). Estimation of damage requires a dynamic link between the flood characteristics (obtainable from the flood inundation model) to the damage estimation model. Apart from flood characteristics, such as flood depths and stage-damage function, a grid-based flood damage model requires various spatial data inputs, such as the exposures distribution, BD, floor area, cost of structure per unit area, and ratio of structural building type in the study area. These spatial data were derived from flood simulation analysis (e.g., flood depths) of remotely sensed data and building information available at the Census and Statistics Department and Disaster Management Centre, Ministry of Disaster Management, Sri Lanka (e.g., urban land cover, building density, unit costs, and floor area). The design of a damage estimation model must be made to directly input the flood inundation model grid outputs (Dutta et al. 2003). Dutta et al. (2003) formulated mathematical models for various urban damage categories (residential and non-residential), which can be used to simulate flood damages in any basin. In this study, their concept for the building structural damage estimation was applied. The model made use of the floor area concept because the economic value of a building structure is defined by the unit floor area and defined as follows:

Table 5 Area covered by urban density types for each secretariat and their total number of buildings

Secretariats	High dense urban (km^2)	Medium dense urban (km^2)	Low dense urban (km^2)	Total number of buildings
Bigiyama	0.88	19.6	13.5	48,090
Thimbirigasyaya	6.93	9.89	1.7	52,763
Sri Jayewardenepura	1.44	12.04	1.4	27,144
Moharagama	0.79	19.38	4.2	49,459
Kolanniwa	1.77	15.88	3.8	44,663
Kelaniya	1.47	16.83	2.6	33,404
Kaduwela	1.35	32.26	22.1	64,791
Colombo	11.8	6.09	1.3	65,831
Homagama	0.50	12.21	34.6	61,505
Dompe	0.29	1.66	25.1	39,369
Padukka	0.17	0.67	13.3	17,007
Hanwella	0.42	1.75	20.8	25,461
Kesbewa	0.71	25.81	11.2	62,653
Dehiwala	3.96	14.55	2.1	22,352
Mahara	0.19	18.93	8.3	52,897
Ja-Ela	0.76	32.44	11.9	52,358
Gampaha	0.21	20.85	13.2	51,111
Watala	3.74	26.30	9.8	43,170

$$D_{s(i,j)} = \sum_{k=1}^{n} \left[N_s(i,j,k)^* FA(i,j,k)^* EC_s(i,j,k)^* C_s(i,j,k) \right] \quad (11)$$

A further modification was done to the damage estimation model using BD and the building ratio concept in order to disaggregate the various global building types within the grid. The above equation is modified as:

$$D_{s(i,j)} = \sum_{k=1}^{n} \left[BD(i,j,k)^* BR(i,j,k)^* FA(i,j,k)^* EC_s(i,j,k)^* C_s(i,j,k) \right] \quad (12)$$

where, for any grid (i, j)

D_s (i, j)	total damage to structure
n	total number of types of building structure
N_s	total number of building units of structure type k
BD (i, j, k)	building density (building units/km^2)
BR (i, j, k)	ratio of building type k
FA	average floor area per building unit of structure type k
EC_s	estimated cost of a building of structure type k per unit area
C_s	Depth-damage function for building structure type k

In Sri Lanka, the replacement cost of residential buildings ranges from 2000 to 4000 LKR/square feet, according to building construction associations. The lower end of the cost is predominantly in the medium and low urban areas, which are most affected by flood. The higher end of the cost is in the high-dense urban area. In order to reflect the construction scenario in the basin, we simulated flood damages based on the price of $165 per square meter. We used the average floor area from the urban and semi-urban area, as reported by the Department of Census and Statistics, and also from the field work carried out in the study area. The 2010 census reported that a 64.5% proportion

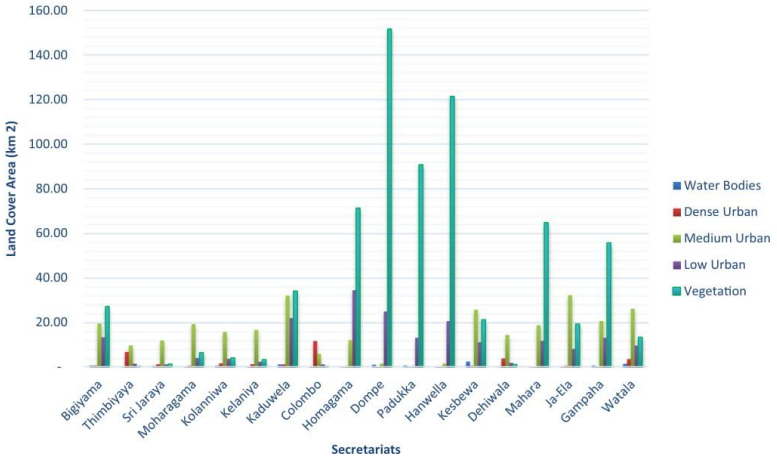

Fig. 8 Graphical representation of five (5) land cover classes in the study area

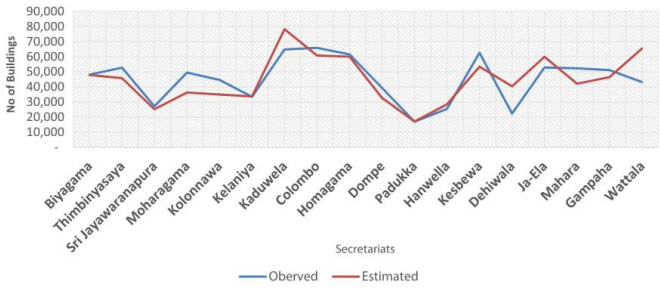

Fig. 9 Estimated number of buildings vs. observed number of buildings

of household units that are within the floor area are greater than or equal to 500 square feet (46 square meter) in Sri Lanka (Census and Statistics Department 2012); whereas about 36.5% occupied less than 500 square feet (46 square meter). The census report shows no much difference between the urban and rural area in terms of floor area occupied by the residential buildings. Quite a large proportion lives between 500 and 750 square feet. Based on the statistics and the field work data, the average floor area of 600 square feet (56 sq m) for both urban and semi-urban areas was used.

Results and discussion

Flood hazards

Figure 11a shows the simulated flood inundation for the flood event (May 2010) in the basin. The extracted maximum flood depths range from 0.8 to 6.2 m. The highest flood heights are experienced along the river's course, mostly in Hanwella, Dompe, and Biyagama. The lowest water heights are experienced in the Colombo area. Simulated inundation extents were compared with observed data from the May 2010 event (Fig. 11b). The observed flood inundation was obtained from ALOS PALSAR 1.5 data product, by Japanese Aerospace Exploration Agency (JAXA) at 6.3-m ground resolution, on May 18, 2010. The extracted observed flood inundation area from PALSAR data as at 18th May 2010 is 53.9km^2; whereas the simulated total inundated area is about 65.4km^2, which extends to all of the administrative boundaries within the basin. Both of the simulated inundation extents match well with the observed inundation. The simulated flood water along the rivers especially in the upstream, agree fully with the observed data. In the downstream part of the inundation map, around the Kolonnawa and Colombo areas, more flood water can be seen in the left bank of the Kelani River compared with very little flood water in the observed data. One of the reasons for this could be the topography data used, which may produce different estimated slopes from what is obtainable on the ground. Another reason could be the resolution used in the simulation, which is 250 m, a rather coarser resolution compared to the observed flood data at 6.3 m. The effect of resolution on the spread and the depths of flood water have been investigated in recent studies (Dutta and Nakayama 2009; Podhorányi et al. 2013). Generally, simulating at coarse resolution would affect the extent/spread of the water and the

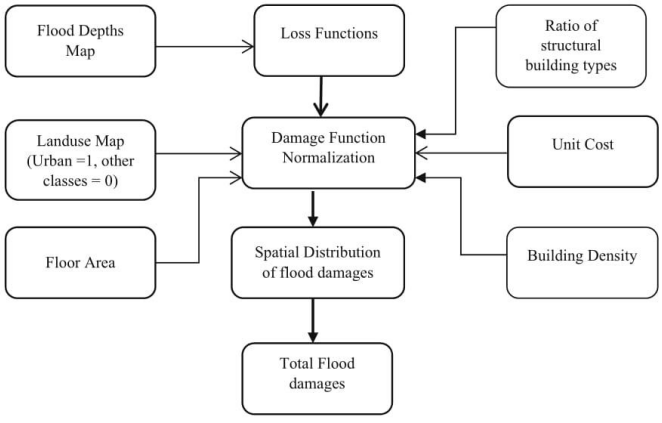

Fig. 10 GIS-based flood damage simulation flow

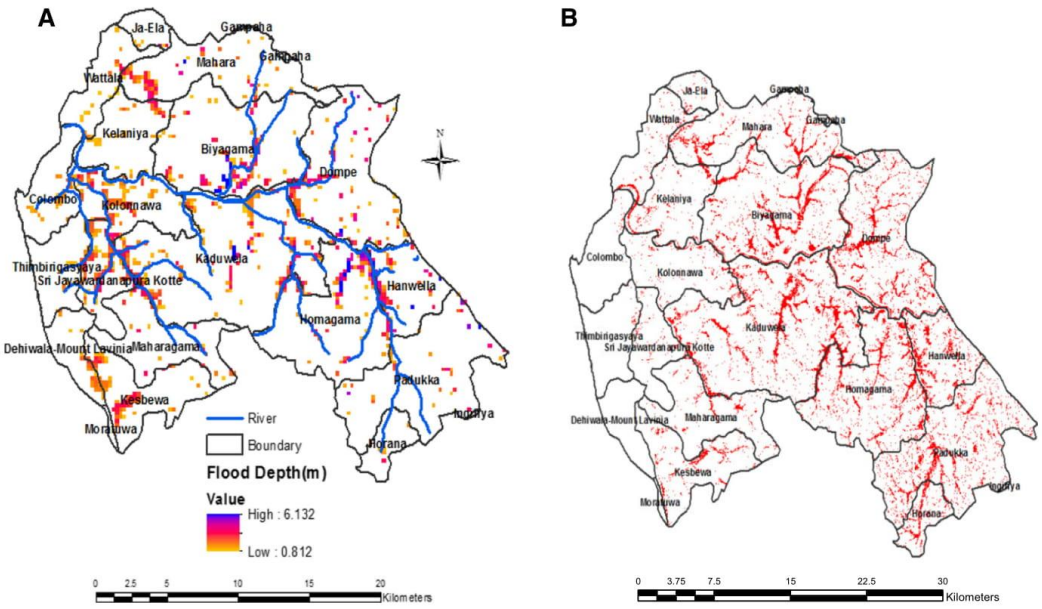

Fig. 11 **a** Simulated flood inundation depths. **b** Observed flood inundation

water heads. The simulation in this study was done at 250-m grid resolution because of available computer resources and the required time to accomplish the simulation over a large basin like the study area. High resolution with accurate topography data would produce higher accuracy in flood simulation.

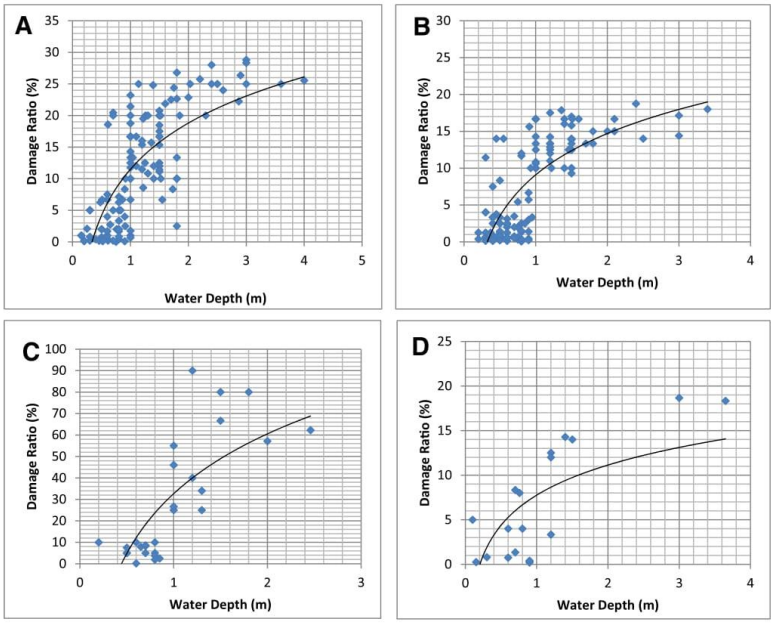

Fig. 12 Flood damage curves for the following. **a** Residential unreinforced masonry (URM). **b** Residential concrete frame with unreinforced masonry walls. **c** Residential wooden structure. **d** Commercial building

Table 6 Derived flood damage coefficients

Building types	C1	C
Unreinforced masonry walls (URM)	10.55	11.487
Concrete frame with unreinforced masonry fill walls	8.0826	9.0925
Wooden	40.211	32.656
Commercial building	4.8745	7.7563

Vulnerability functions

Figure 12 shows the degree of flood damage expected at a given flood depth for each of the global building structural types. The damage ratio for the building categories slightly varies. The wooden and unreinforced masonry walls show maximum damage ratio as explained by the applied model at 70 and 26%, respectively, while the concrete frame with unreinforced masonry walls revealed maximum damage at 19%. The commercial structures are predicted at 14%. The degree of damages in each of the building categories shows the responses of different building materials to water depths. From the model, wooden and unreinforced masonry walls are more vulnerable to flood than the concrete frame with unreinforced masonry. Wooden structures are typically highly vulnerable to water and are expected to have higher damage ratio with respect to flood water height. The flood damage coefficients (C1 and C) for all the building as defined by the logarithm model in Eq. 9 as listed in Table 6.

Flood damage estimates and model validation

Simulated damages are $64,065, $248,096, and $331,012 for residential wooden, concrete frame with unreinforced masonry (CFURM), and unreinforced masonry walls (URM) structures, respectively (Fig. 13). The wooden (despite the highest vulnerability to flood) accounts for the lowest damages in the basin. This is because of the scanty distribution of wooden structures in the study area. Expectedly, URM (the predominant structures with relatively high vulnerability) showed the highest damages, followed by the CFURM. Damages to commercial buildings, mostly made up of concrete structures, are estimated to be $42,358.

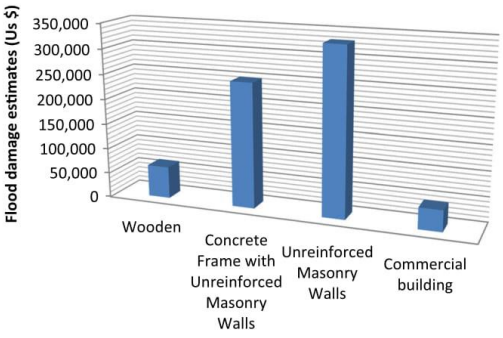

Fig. 13 Estimated total flood damages for different building types

Models validation

In 2010, between May 12 and May 21, heavy rainfall resulted in a devastating flood that affected about five districts (Colombo, Gampaha, Kalutara, Galle, and Matara) out of Sri Lanka's 25 districts (DMC 2010). According to DMC (2010), the value of damages and losses was estimated at LKR 5,059 million or $46 million. Kelani River basin, which is comprised of mainly Colombo and Gampaha districts, accounts for a total of LKR 90 million ($750,188) worth of damages to house structures, LKR 28 million worth of damages to household goods, LKR 26 million for the cost of shelter, and LKR 116 million for clean-up costs (Table 7).

Table 8 shows the simulated damages for all of the three (3) global building structural types in the study area, in comparison with the post-flood survey damages estimated by the Disaster Management Centre, Ministry of Disaster Management, Sri Lanka (DMC). Damages to commercial structure cannot be verified in this study because of lack of detailed observed damage for commercial building. It can be observed from the aggregated simulated damages to residential structures that they are lower than the damages from the post-flood field survey by about 17% (Fig. 14). This difference can be attributed to the fact that the extent of damages in the lower Kelani basin, though comprised of two major Districts (Colombo and Gampaha), does not fully encompass all of the secretariats in the districts, especially Gampaha in the northern part, which recorded higher damages according to the observed damage reports (see Fig. 4). Assuming that all of the secretariats are within the lower basin, it is expected that the simulated damages will be a slightly higher (about 30%) than the observed damages. This expected higher damage can be attributed to the difference in the extent of the simulated inundation and the observed map.

Since the simulated lower Kelani basin covers most parts of Colombo district (see Fig. 4), it will be much better to compare the observed and estimated damages for Colombo district. Figure 15 shows the comparison between the observed and the estimated damages for Colombo district. It can be observed that the estimated damages exceed the observed damages with about 30%. The reason, as earlier mentioned, could be the grid resolution (250 m) used in the simulation. Also, some other factors, such as the detention basin, buildings, and some locally elevated highways, which were not considered in the simulation, can be a major cause of the large difference. Estimation of property exposure is an important factor that can be attributed to the difference. The study made use of Landsat-8 OLI with 30-m resolution to extract the build-up areas in the basin and the estimation of urban density.

Table 7 Observed damages (May 2010 flood event) to housing by district (LKR million) adapted from DMC (2010)

	Damages to houses structures	Damages to household goods	Shelter costs	Clean-up costs
Colombo	44	13	11	54
Gampaha	46	15	15	62
Total	90	28	26	116

Higher resolution imagery, as suggested by Komolafe et al. (2015), would be necessary, especially when the flood heights are simulated at coarse resolution. Despite the uncertainty sources, the performances of the loss models are near accurate and can be used for future approximate estimation of flood damages for risk planning and prevention.

From the results, it clearly shows that the empirically generated loss functions through field survey can provide more accurate flood damage forecast if past observed/surveyed flood damage data are available for model calibration and validation. The loss functions were able to predict of about 70% of the observed total flood damages of May 2010 flood event in the Kelani River basin. Meaning that, by using the three loss functions and the spatial data components in this study, 70% of the future flood damages can be predicted. However, more accurate results can be achieved if higher resolution remote sensing data is used for the mapping of the urban property distribution and ambiguities in the inundation modeling are reduced.

Conclusions

In this study, four vulnerability (damage) curves for floods were developed for global building types using an empirical approach applied to the Kelani River basin in Sri Lanka. This was done with the aim of differentiating economic losses associated with each element at risk (de Moel et al. 2012) and

Table 8 Simulated damages based on global building types vs. the observed total damages

Residential building types in the River basin	Simulated flood damages (USD)	Observed flood damages (USD) to residential structures
Wooden	$64,065	
Concrete frame with unreinforced masonry walls	$248,096	
Unreinforced masonry walls	$331,012	
Total damages to residential structures	*$643,173*	*$750,188*
Commercial building structure	$42,358	

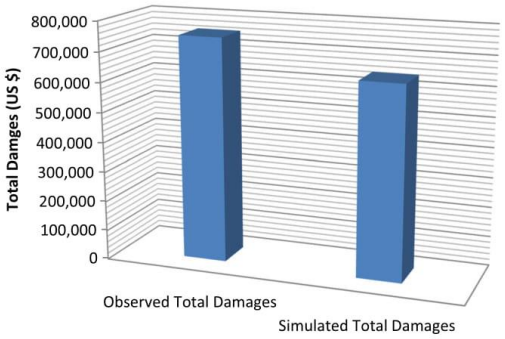

Fig. 14 Simulated vs. observed total damages for residential structures

generating input data to the regional or global risk model for risk comparison and mobilization of international supports for risk reduction and management. The flood inundation was simulated using Flo-2D, a grid-based hydrodynamic flood model, which considered major physical occurrences in the river basin. An event-based (May 2010) flood modeling was applied in order to validate the established loss functions. A modified integrated mathematical model, which provides a dynamic link between the simulated flood and the established detailed loss functions, was used to provide spatial distribution of flood losses for each residential building structure in the study area. This paper has demonstrated the possibility of differentiating economic losses (in each structural damage category), instead of the usual aggregated losses that are more commonly documented. The results of the inundation simulation, to some extent, match with the observed flood map and show the capability of the Flo-2D model in estimating flood inundation parameters over a relatively large basin like the study area.

The slight difference in the flood extent of the simulated and the observed flood map could be as a result of the inability to incorporate other factors, such as buildings, detention basin, street, and groundwater. Due to the size of the river basin and

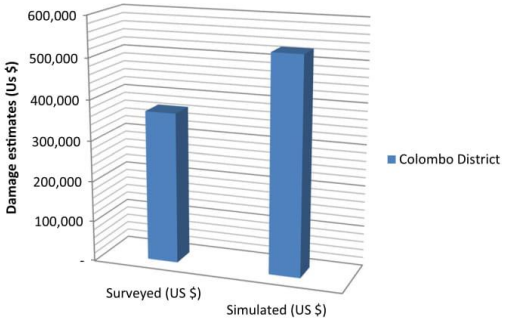

Fig. 15 Simulated vs. observed total damages for residential structures for Colombo District

in order to ensure a faster grid simulation, a grid size of 250 m was used in the simulation. This, in addition to previous factors, could have resulted in some level of ambiguity in the simulated model. Further improvement in the future can consider and/or mitigate these factors for enhanced simulation. The maximum vulnerability index predicted by the model for the building types in the study areas showed 0.7, 0.26, 0.19, and 0.14, for wooden, unreinforced masonry walls (URM), concrete frame with unreinforced masonry walls (CFURM), and commercial structures, respectively. This revealed the damage responses of the building structures to flood water, which is dependent on the materials of the buildings and the water depths. As expected, woods are more susceptible to flood water, and hence has the highest vulnerability index, followed by the URM, CFURM, and commercial structures.

It is intended that the empirically established loss functions can be incorporated at the regional scale for developing regional-specific functions. Apart from providing input data for regional flood-risk modeling, the established model can also be transferable and applicable to other countries for comparing flood risk associated with similar building materials and types. This can be done by normalizing the floor area and country or the regional replacement cost. The generalized loss functions can be employed for estimating future losses to flood and to evaluate the influence of climate change on potential flood damages, as well as for understanding the relative impact on a given country's economy. This is very essential for decision making by governmental agencies and investors for collaborating and planning for disaster risk reduction.

Acknowledgements We appreciate the Japan Foundation for UNU and the CECAR ASIA for providing funds for this research. FLO-2D Software, INC is appreciated for supporting this research and Flo-2D software, respectively. Much thanks to the Japan Aerospace Exploration (JAXA) for providing satellite data for this study.

References

Ahmad S, Avtar R, Sethi M, Surjan A (2016) Delhi's land cover change in post transit era. Cities 50:111–118

Ahmed I, Gerlach RM Distributed flow guided dydraulic modeling of a desert river system for flood control, *in* Proceedings River Flow 2012, Costa Rica San Jose, 2012, 1, Taylor and Francis Group, LLc, p. 1007–1015

Avtar R, Takeuchi W, Sawada H (2013) Full polarimetric PALSAR-based land cover monitoring in Cambodia for implementation of REDD policies. Int J Digital Earth 6(3):255–275

Bhatti SS, Tripathi NK (2014) Built-up area extraction using Landsat 8 OLI imagery. GI Sci Remote Sens 51(4):445–467

Cammerer H, Thieken A (2013) Historical development and future outlook of the flood damage potential of residential areas in the Alpine Lech Valley (Austria) between 1971 and 2030. Reg Environ Chang 13(5):999–1012

Cammerer H, Thieken AH, Lammel J (2013) Adaptability and transferability of flood loss functions in residential areas. Nat Hazards Earth Syst Sci 13(11):3063–3081

Census (2012) Census of Pupolation and Housing: Department of Census and Statistics, Ministry of Finance and Planning

Chow VT (1959) Open-channel hydraulics. Blackburn Press, Calwell

de Moel H, Asselman NEM, Aerts JCJH (2012) Uncertainty and sensitivity analysis of coastal flood damage estimates in the west of the Netherlands. Nat Hazards Earth Syst Sci 12(4):1045–1058

De Silva MMGT, Weerakoom SB, Herath S, Ratnayake UR (2012) Event Based Flood Modeling in Lower Kelani Basin, in Proceedings SAITM Research Symposium on Engineering Advancements, Malabe, Sri Lanka

DMC (2010) Integrated Post Flood Assessment: Disaster Management Centre, Ministry of Disaster Management

Dutta D, Herath S (2001) GIS Based Flood Loss Estimation Modeling in Japan, in Proceedings Proceedings of the US-Japan 1st Workshop on Comparative Study on Urban Disaster Management, Port Island, Kobe, Japan, February 2001

Dutta D, Herath S, Musiake K (2003) A mathematical model for flood loss estimation. J Hydrol 277(1–2):24–49

Dutta D, Kamrujjaman Serker NHM (2005) Urban building inventory development using very high resolution remote sensing data for urban risk analysis. Int J Geoinform 1(1):109–116

Dutta D, Nakayama K (2009) Effects of spatial grid resolution on river flow and surface inundation simulation by physically based distributed modelling approach. Hydrol Process 23(4):534–545

Flo-2D (2009) Flo-2D Reference manual, *in* FLO-2D Software, I., ed.: Nutrioso

Freni G, La Loggia G, Notaro V (2010) Uncertainty in urban flood damage assessment due to urban drainage modelling and depth-damage curve estimation. Water Sci Technol—WST 61(12):2979–2993

Giang NT, Chen J, Phuong TA (2009) A method to construct flood damage map with an application to Houng River basin, Central Vietnam. VNU J Sci, Earth Sci 25:10–19

Heisten M, Davdge D (2005) Flood damage estimation in the Upper Themes River Watershed. University of Western Ontario and University of Waterloo, Waterloo

Herath S, Dutta D, Musiake K (1999) Flood damage estimation of an urban catchment using remote sensing and GIS, *in* Proceedings International Conference on Urban Storm Drainage, Volume 4, p. 2177–2185

Herath S, Hirose N, Matsuda S (1992) A process model for basin hydrological modelling and its application, *in* Proceedings Japan Annual Conference of Society of Water Resources and Hydrology,, p. 146–149

Herath S, Hirose N, Musiake K (1990) A computer package for the estimation infiltration capacities of shallow infiltration facilities, *in* Proceedings 5tt International Conference on Urban Storm Drainage, Japan, p. 111–118

Herath S, Ni G, Babar B, and Musiake K (1995), Investigation of scaling effect in hydrologic modeling using distributed hydrologic models, *in* Proceedings 2nd Study Conference on GEWEX Asian Monsoon Experiment, Thailland, 6–10, March 1995, p. 207–211

Herath, S., and Wang, Y., 2009, Incorporating wind damage in potential flood loss estimation: Global Environmental Research p. 151–159

Islam MM, Ado KS (2000) Flood damage and management modelling using satellite remote sensing data with GIS: case study of Bangladesh, *in* Proceedings Remote Sensing and Hydrology 2000 (Proceedings of a symposium held at April 2000). IAHS Publ. no. 267, 2001, Santa Fe, New Mexico, USA,

James L, Hall B (1986) Risk information for floodplain management. J Water Resour Plann Manag 112(4):485–499

Jongman B, Kreibich H, Apel H, Barredo JI, Bates PD, Feyen L, Gericke A, Neal J, Aerts JCJH Ward PJ, (2012) Comparative flood damage

model assessment: towards a European approach: Nat. Hazards Earth Syst. Sci.,, v. 12, p. Nat. Hazards Earth Syst. Sci.,

Jonkman SN, Bočkarjova M, Kok M, Bernardini P (2008) Integrated hydrodynamic and economic modelling of flood damage in the. Netherlands: Ecological Economics 66(1):77–90

Kelman, I., and Spence, R., 2004, An overview of flood actions on buildings: Eng Geol, v. 73, no. 3–4, p. 297–309

Kimura K, Ishimi K, Sato S, Fukuda T, Mikami T, Kikuchi S (2006) Verification of tsunami wave source model and formulation of vulnerability function for buildings based on the investigation of actual damage due to the Sumatran earthquake and tsunami: subject area bein the damage at Matara city. Sri Lanka: Costal Eng Committee 53:301–305

Komolafe AA, Srikantha H, Avtar R, (2015) Sensitivity of flood damage estimation to spatial resolution: journal of flood risk management, p. https://doi.org/10.1111/jfr1113.12224

Kreibich H, Thieken AH, Petrow T, Muller M, Merz B (2005) Flood loss reduction of private households due to building precautionary measures—lessons learned from the Elbe flood in August 2002. Natural Hazards Earth Syst Sci 5(1):117–126

Maktav D, Erbek FS, Jurgens C (2005) Remote sensing of urban areas. Int J Remote Sens 26(4):655–659

Masqsood T, Wehner M, Ryo H, Edwards M, Dale K, Miller V (2013) GAR 15 Regional Vulnerability Functions: Reporting on the UNISDR/GA SE Asian Regional Workhop on Structural Vulnerability Models for GAR Global Risk Assessment, 11–14 November, 2013, : Geoscience Australia

Merz B, Kreibich H, Schwarze R, Thieken AH (2010) Assessment of economic flood damage. Nat Hazards Earth Syst Sci 10:1697–1724

Ministry of Irrigation Resources, S. L., 2009, Proposed Kaluganga Multipulse development Project.: Department of Irrigation, Water Resources abd Planning, Ministry of Irrigation and Water Management

Moel, H., and Aerts, J. C. J. H., 2011, Effect of uncertainty in land use, damage models and inundation depth on flood damage estimates: Nat Hazards, v. 58, no. 1, p. 407–425

Murao O, Nakazato H (2010) Vulnerability functions for Buildings Based on Damage Survey Data in Sri Lanka after the 2004 Indian Ocean Tsunami, in Proceedings International Conference on Sustainable Built Enviroment (ICSBE), Kandy,

Nash JE, Sutcliffe JV (1970) River flow forecasting through conceptual models part I—a discussion of principles. J Hydrol 10(3):282–290

Niroshine MAC (2012) Adaptation to Extreme Floods Under Future Climate Change Scenarios for Colombo, Sri Lanka, International Forum for Sustainable Asia and the Pacific: Yokohama, Japan

Niroshinie MAC, Babel MS, Herath S (2011) A methodology to analyze extreme flooding under future climate change scenarios for Colombo, Society for Social Management Systems Internet Journal, Society for Social Management Systems

Notaro V, De Marchis M, Fontanazza CM, La Loggia G, Puleo V, Freni G (2014) The effect of damage functions on urban flood damage appraisal. Procedia Eng 70(0):1251–1260

Peris N (2006) Vulnerability functions for tsunami loss estimation, *in* Proceedings 1st European Conference on Earthquake Engineering and Seimology, Volume 1121

Podhorányi M, Unucka J, Bobál P, Říhová V (2013) Effects of LIDAR DEM resolution in hydrodynamic modelling: model sensitivity for cross-sections. Int J Digital Earth 6(1):3–27

Richards JA (2013) Remote sensing digital image analysis: an introduction. Springer, New York

Xu H (2007) Extraction of urban built-up land features from Landsat imageries using a thematic-oriented index combination technique. Photogramm Eng Remote Sens 73(12):1381–1390

7.2. Annex 02 - Annexes on content damage survey

7.2.1. Initial composition of the survey locations

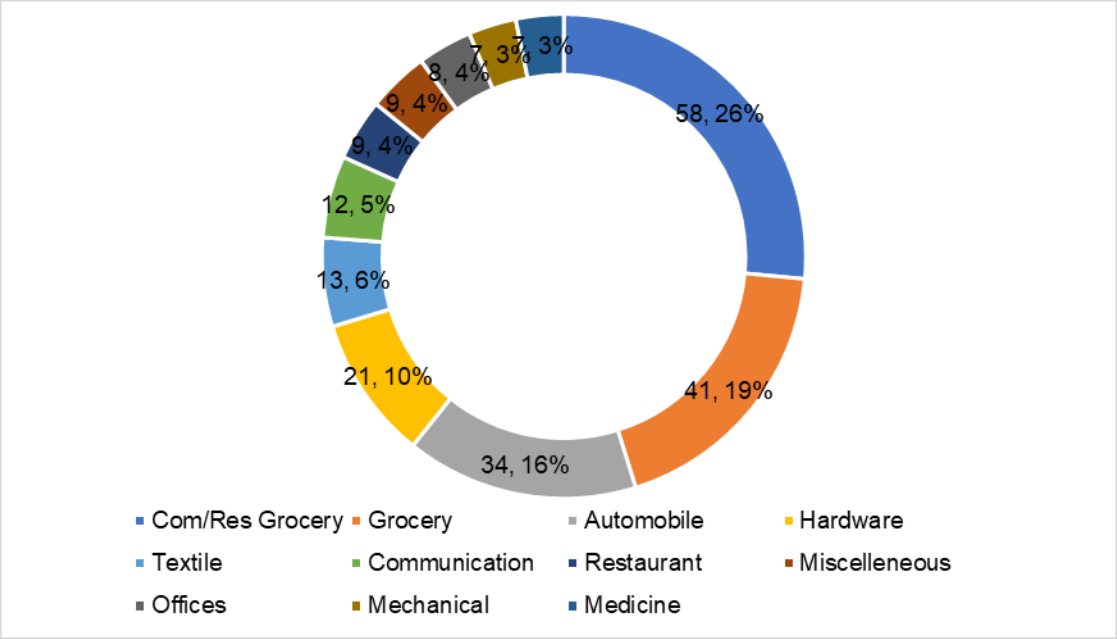

Figure 9. Composition of the survey locations (Number, percentage)

7.2.2. Surveyed flood depths comparison with the modelled flood depths

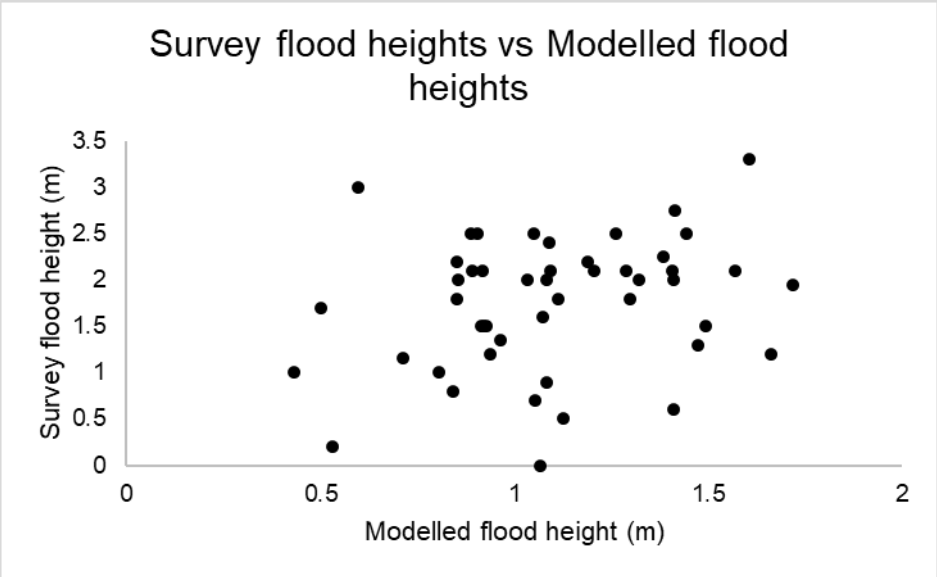

Figure 10. Survey flood heights vs Modelled flood heights

Theoretically, the above graph should show a linear relationship between the variables, however it has been different in this case. This could be caused by the lack of clear memory of the respondents on the incidents, exaggeration of details by the respondents and the discrepancies in the FLO-2D model output.

7.2.3. Damage (LKR/m^2) vs the flood height graphs for the initially identified building types

The results of the analysis are shown in this section, for each type of building use. It should be noted that only the damage to the building content is considered in deriving the relationships.

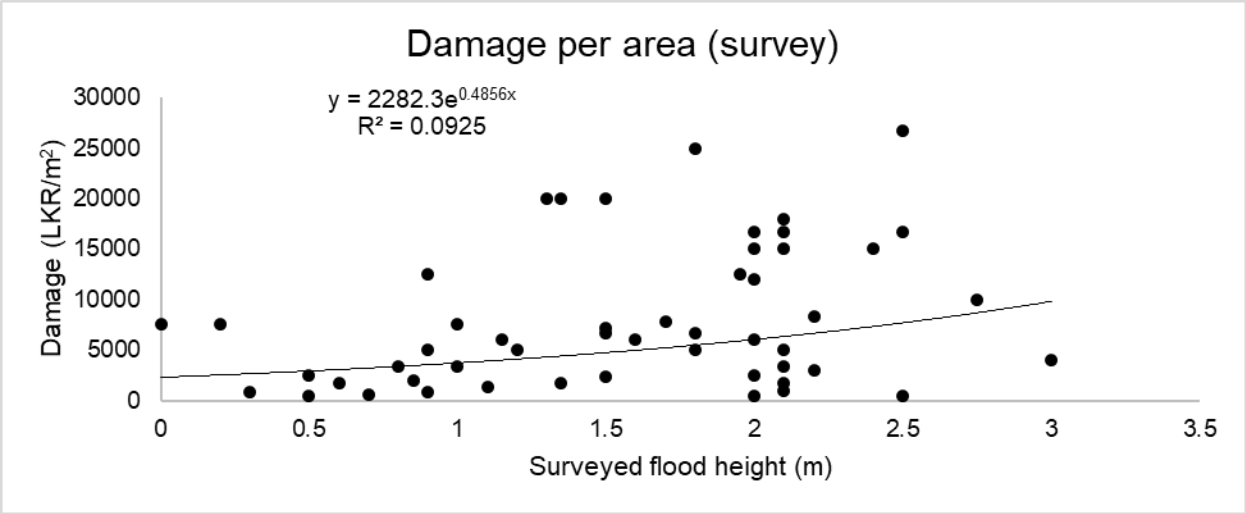

Figure 11.Groceries in residential buildings (Com/Res Grocery)

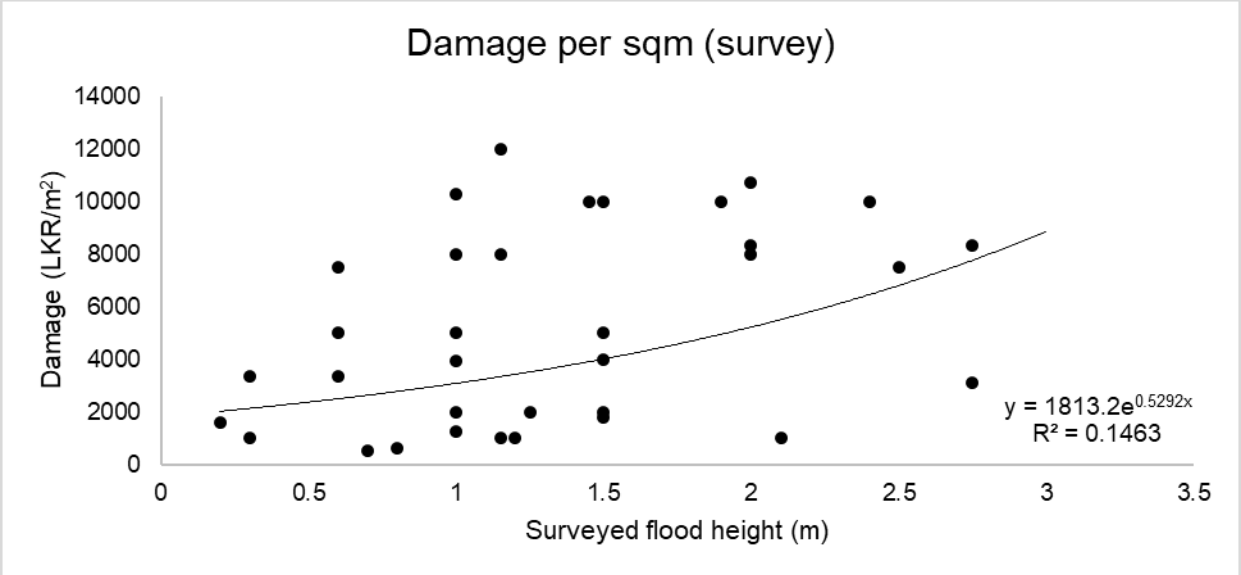

Figure 12. Grocery

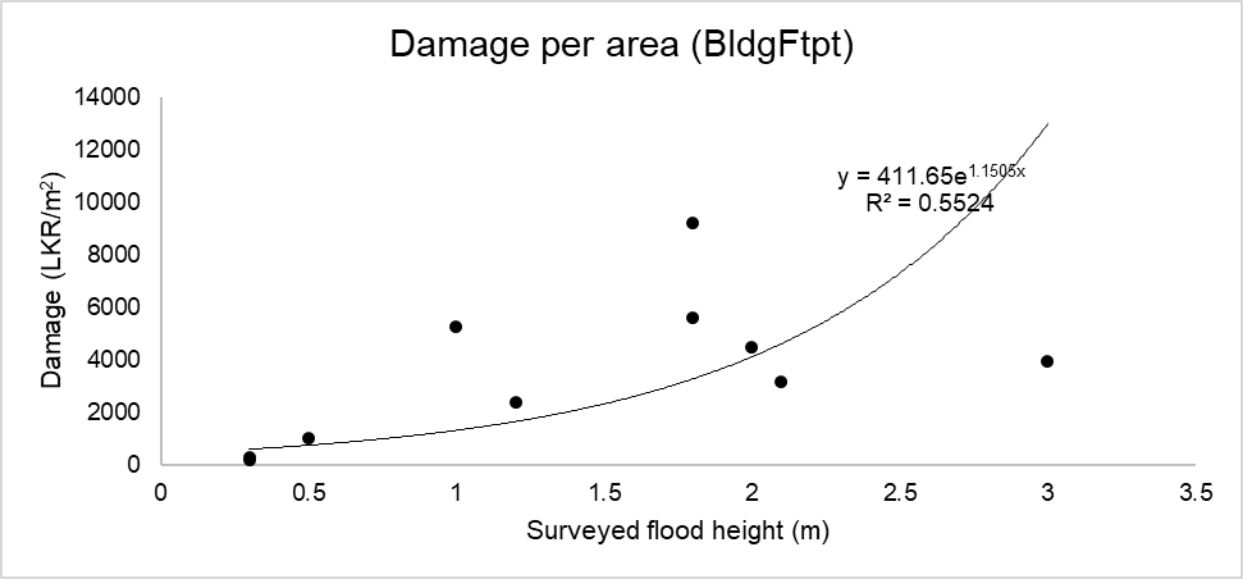

Figure 13. Communications and bookshops

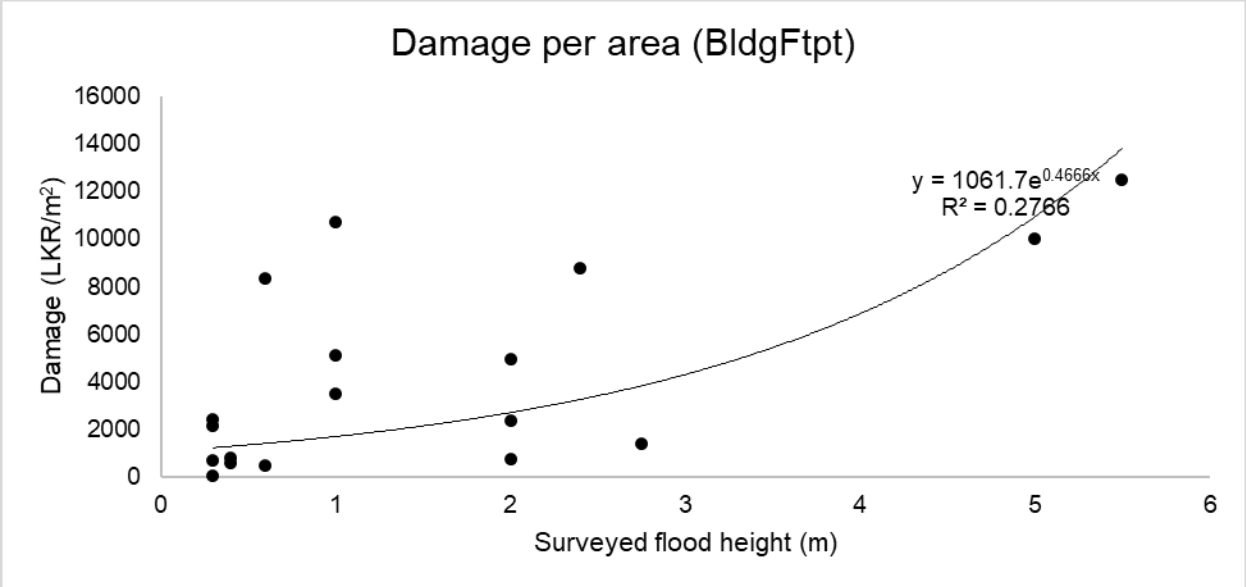

Figure 14. Garages

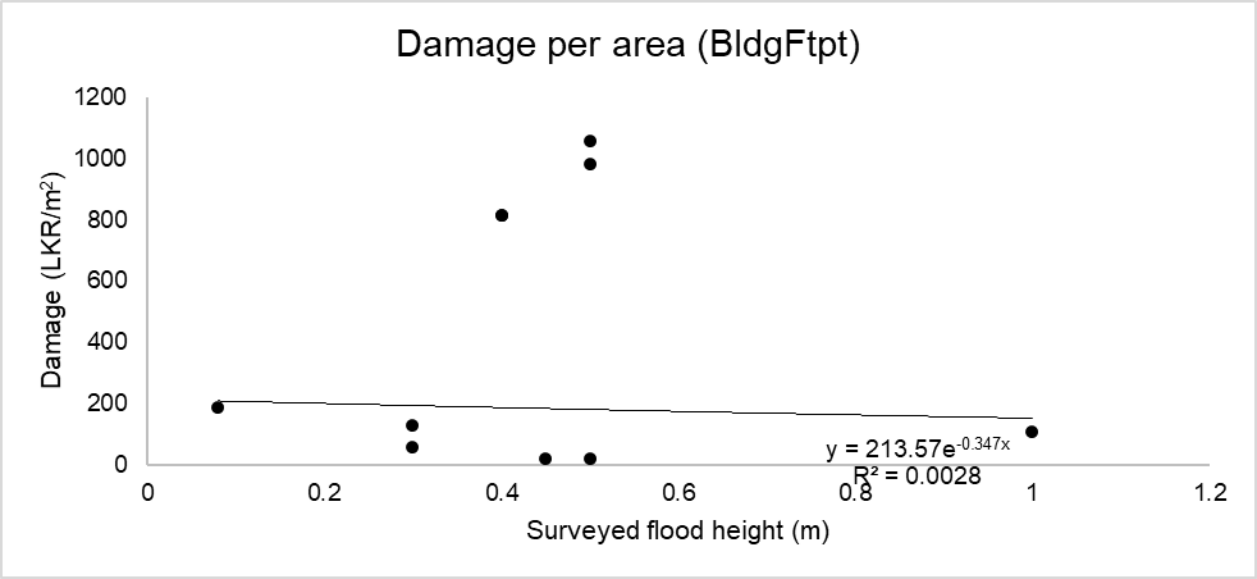

Figure 15. Spare parts centers and service centers

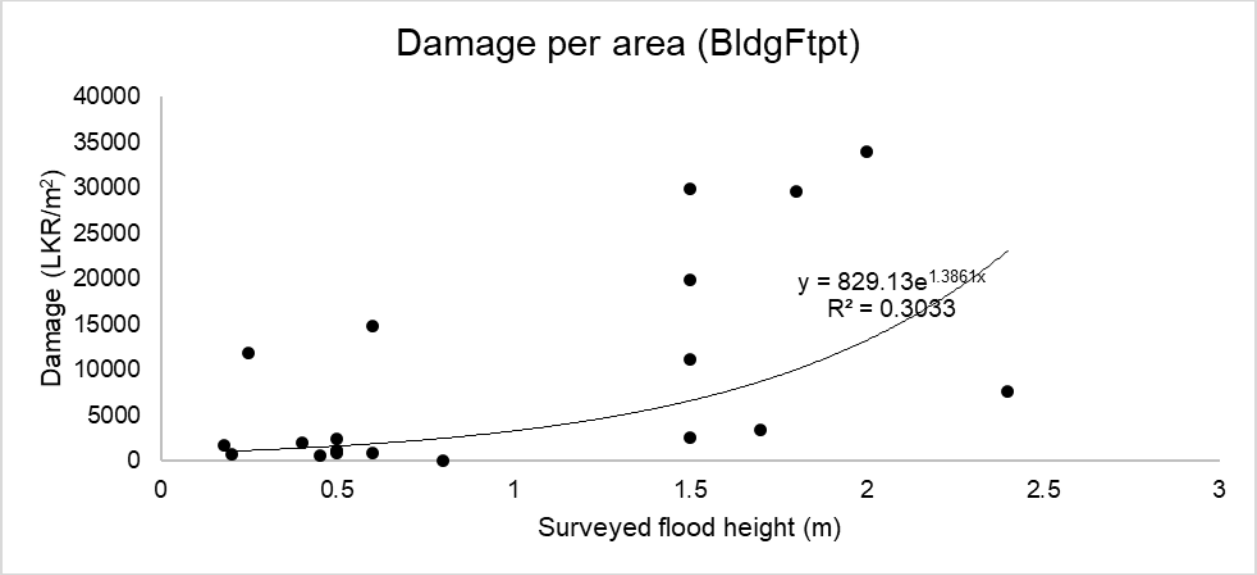

Figure 16. Hardware stores

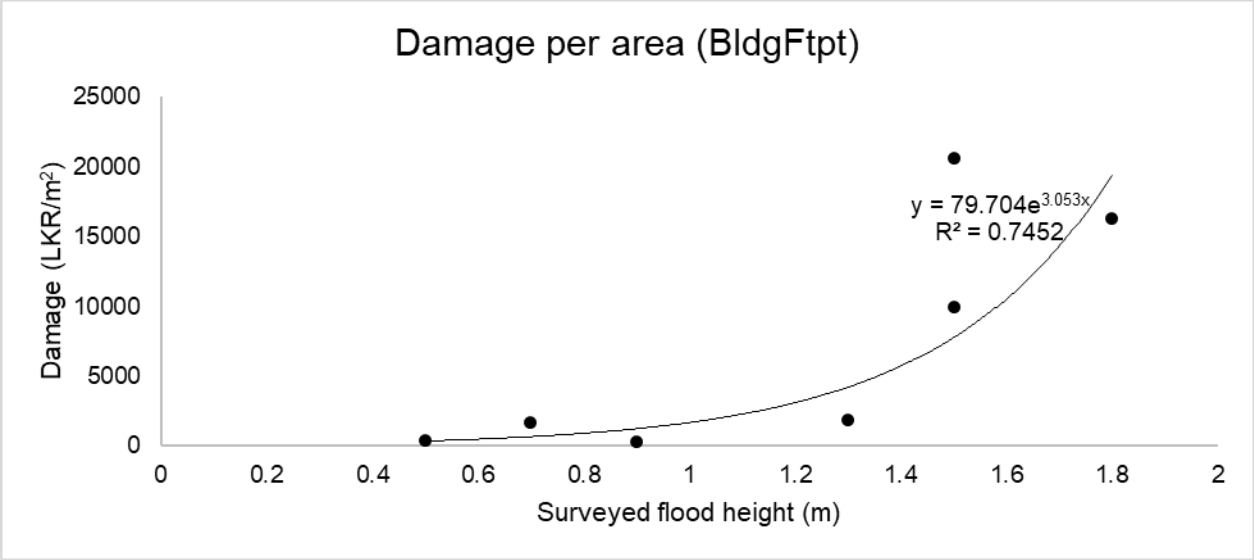

Figure 17. Mechanical shops (iron-work/lathe/glass/welding and workshops)

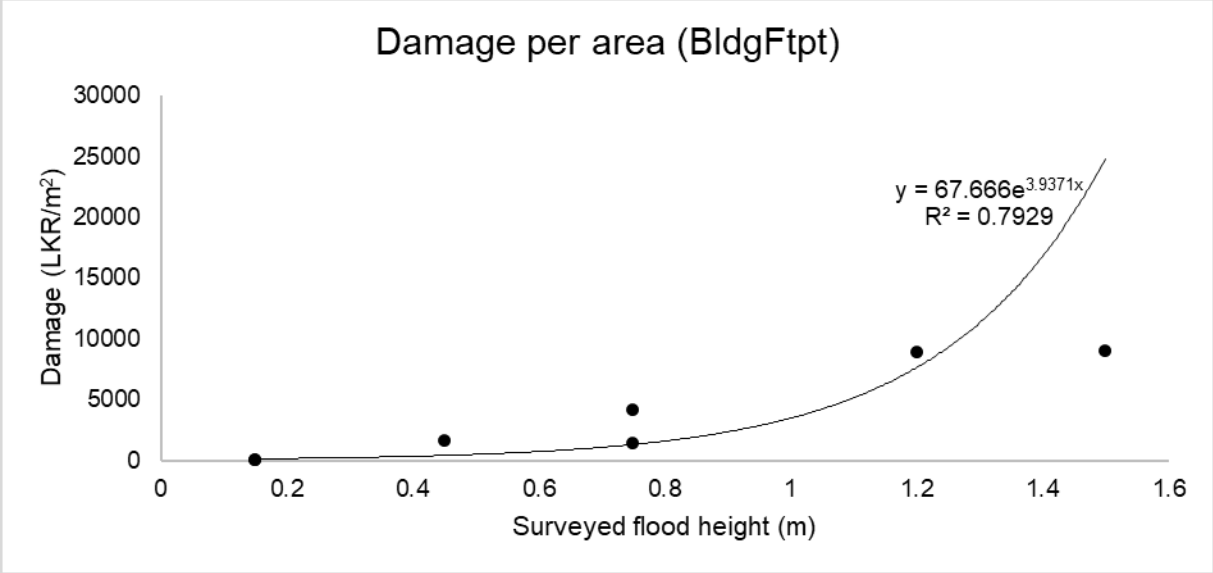

Figure 18. Medicine related (Pharmacies/dispensaries)

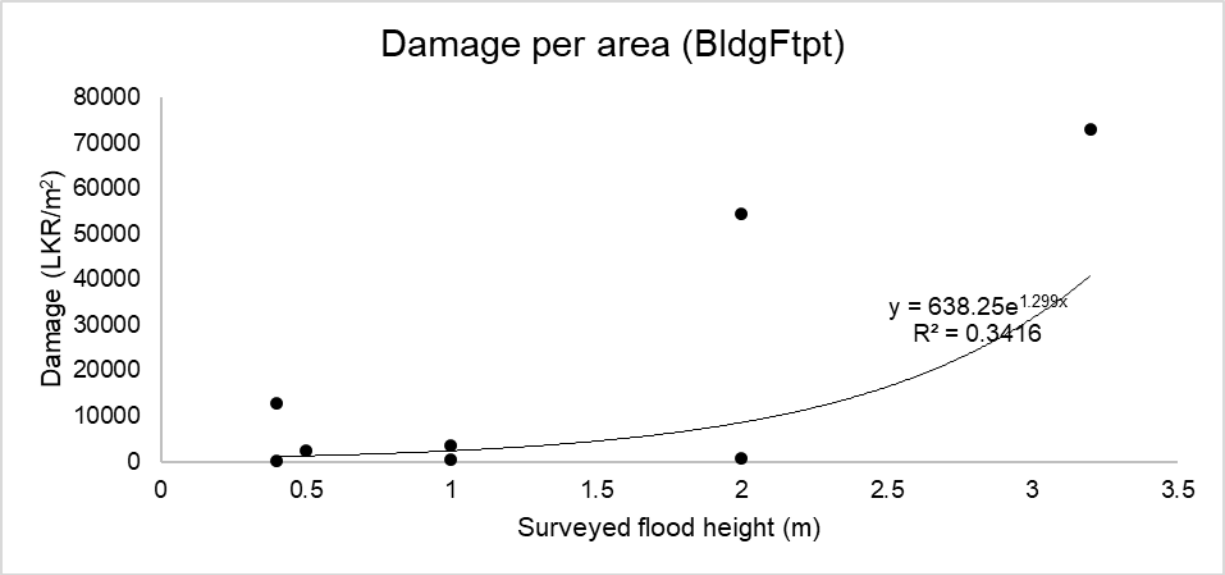

Figure 19. Offices

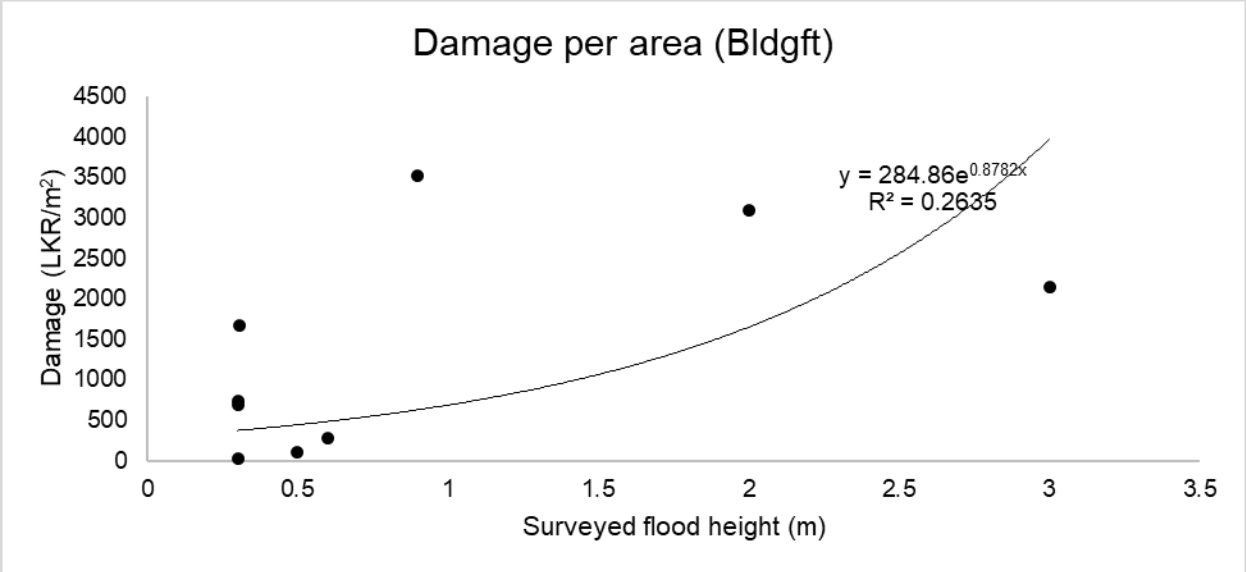

Figure 20. Restaurants/Tea shops

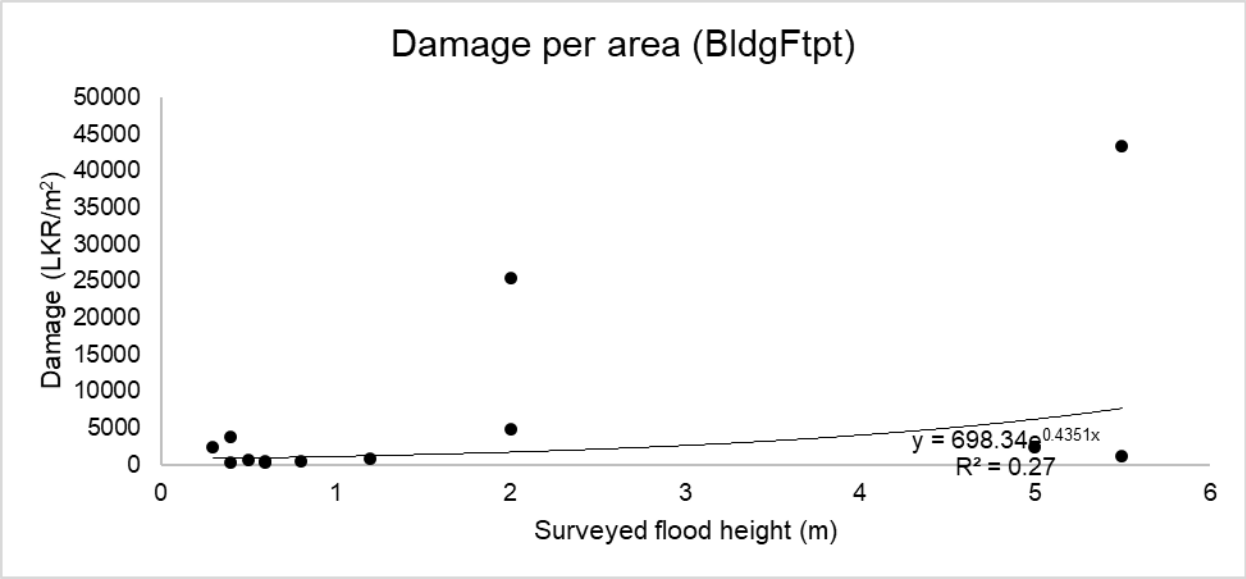

Figure 21. Textile shops

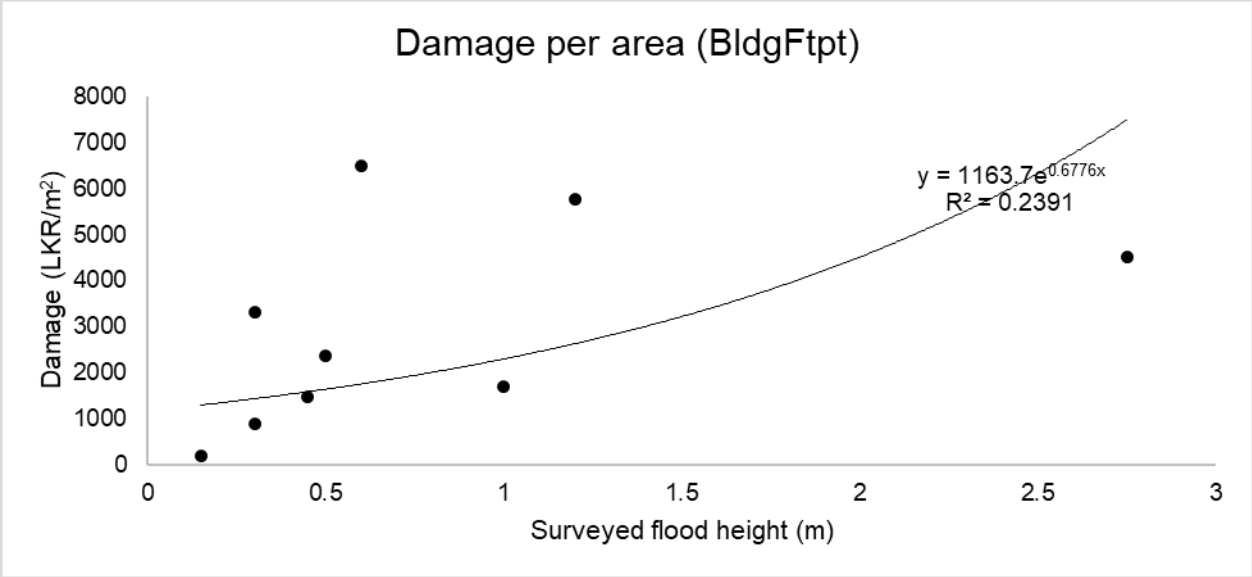

Figure 22. Miscellaneous (beer shops/salons/timber workshops)

The relationships derived in the graphs can be seen as reasonable fits for particular couples of variables, which are not consistent for all of the building uses. Therefore, the curves should be used particularly for a specified building use. Furthermore, the fits could be approximated to logarithmic relations, if required and justified (the approximation to the exponential curves are done upon the recommendations of the PHRD study).

7.3. Annex 03 - Results of the sensitivity analysis

Calculated below are the content damage for different flood scenarios for the Metro Colombo region. Here, the content damage is calculated in two methods: using the damage curves for the identified building clusters and using the damage curves for individual building (lump) categories. For these calculations, a plinth height of 0.3 m is assumed for all types of buildings.

Scenes	Educational buildings	Health sector buildings	Industrial buildings	Office buildings	Residential buildings	Shops	Vacant buildings	Warehouses
'HK10Clustered'	33,659,401	35,673,107	170,401,541	127,442,686	607,479,071	72,506,431	42,915,380	223,513,440
'HK10Lump'	26,734,601	5,765,948	27,542,496	14,617,786	482,501,469	57,589,572	34,086,333	36,127,127
'HK25Clustered'	71,327,816	77,894,529	424,773,255	321,238,703	1,564,682,984	145,574,543	124,445,811	459,170,103
'HK25Lump'	56,653,435	12,590,319	68,657,336	36,846,356	1,242,778,353	115,625,269	98,843,383	74,216,999
'HK50Clustered'	168,373,463	143,147,361	1,107,053,173	740,034,078	3,472,866,348	366,519,344	256,033,891	1,242,361,067
'HK50Lump'	133,733,732	23,137,324	178,936,222	84,882,547	2,758,388,226	291,114,757	203,359,645	200,806,431
'HK100Clustered'	295,589,783	247,234,598	1,475,564,659	1,424,917,237	5,513,648,073	618,396,254	359,692,702	1,821,426,121
'HK100Lump'	234,777,643	39,961,247	238,499,805	163,439,236	4,379,316,795	491,172,643	285,692,570	294,402,399

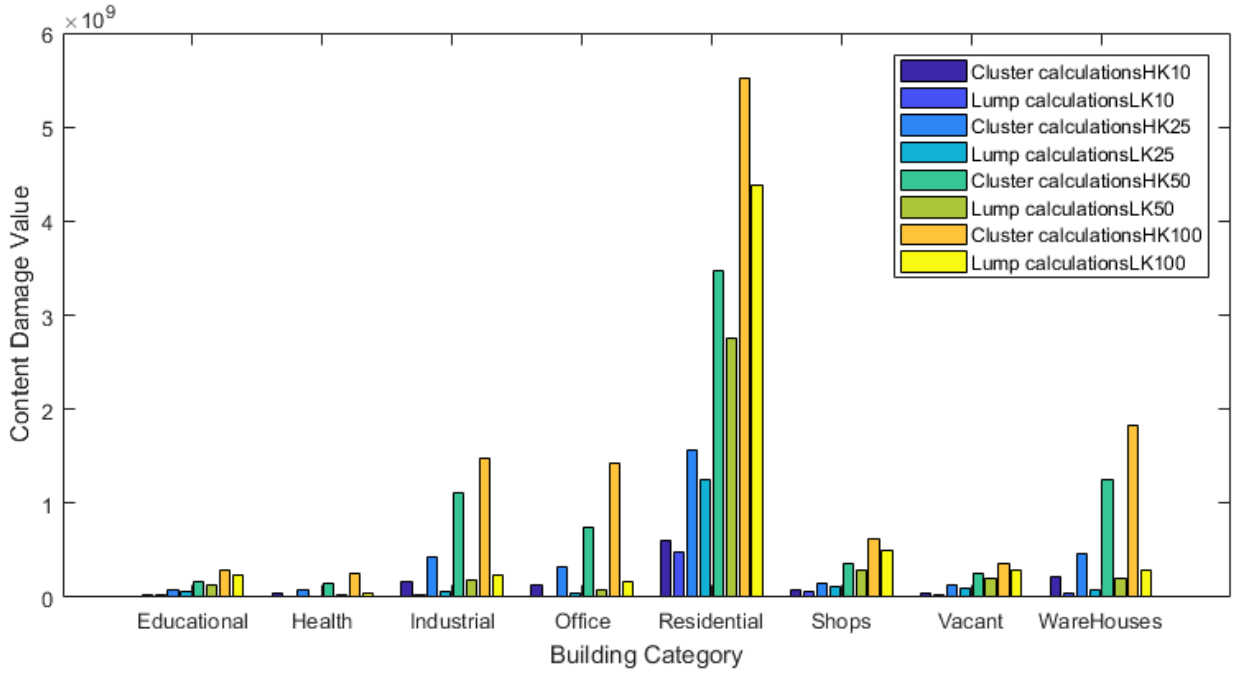

Figure 23. Comparison of clustered and lumped calculations for building content damage

7.4. Annex 04 - Comparison between the building properties in the vector format and the raster format

Structural building uses are shown in blue colour, while the building content use is shown in purple colour.

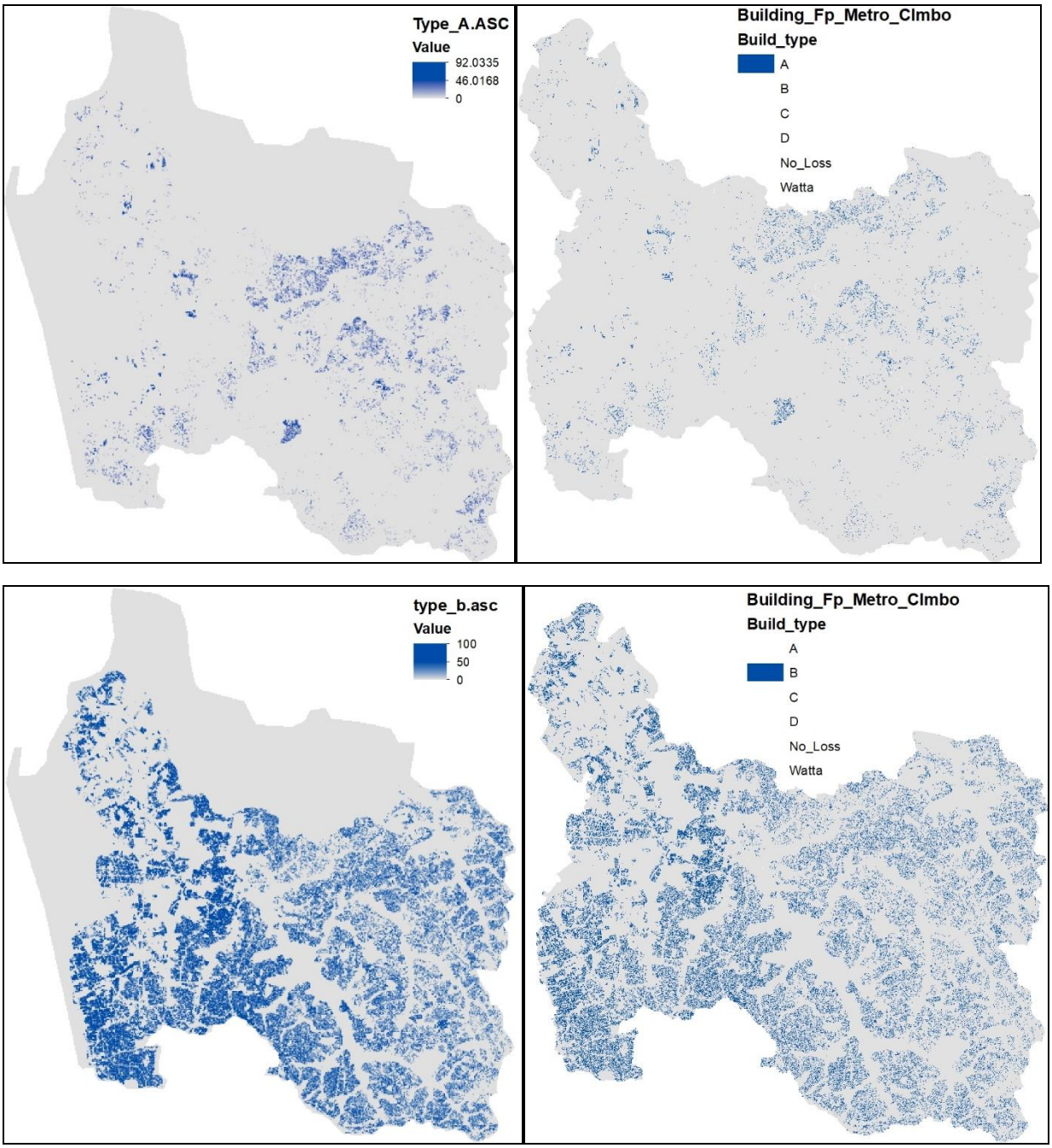

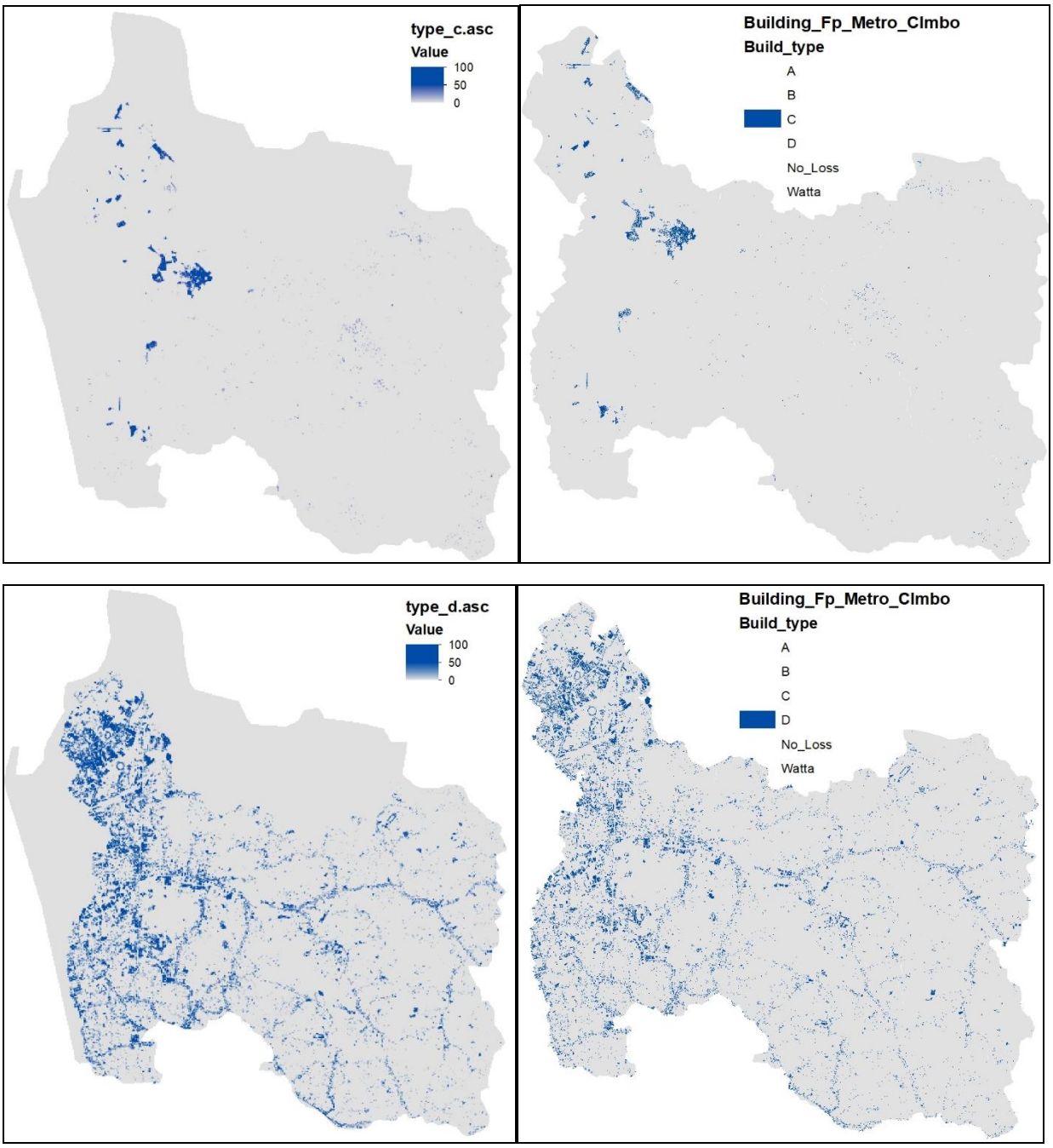
type_c.asc
Value
100
50
0
Building_Fp_Metro_Clmbo
Build_type
A
B
C
D
No_Loss
Watta
type_d.asc
Value
100
50
0
Building_Fp_Metro_Clmbo
Build_type
A
B
C
D
No_Loss
Watta

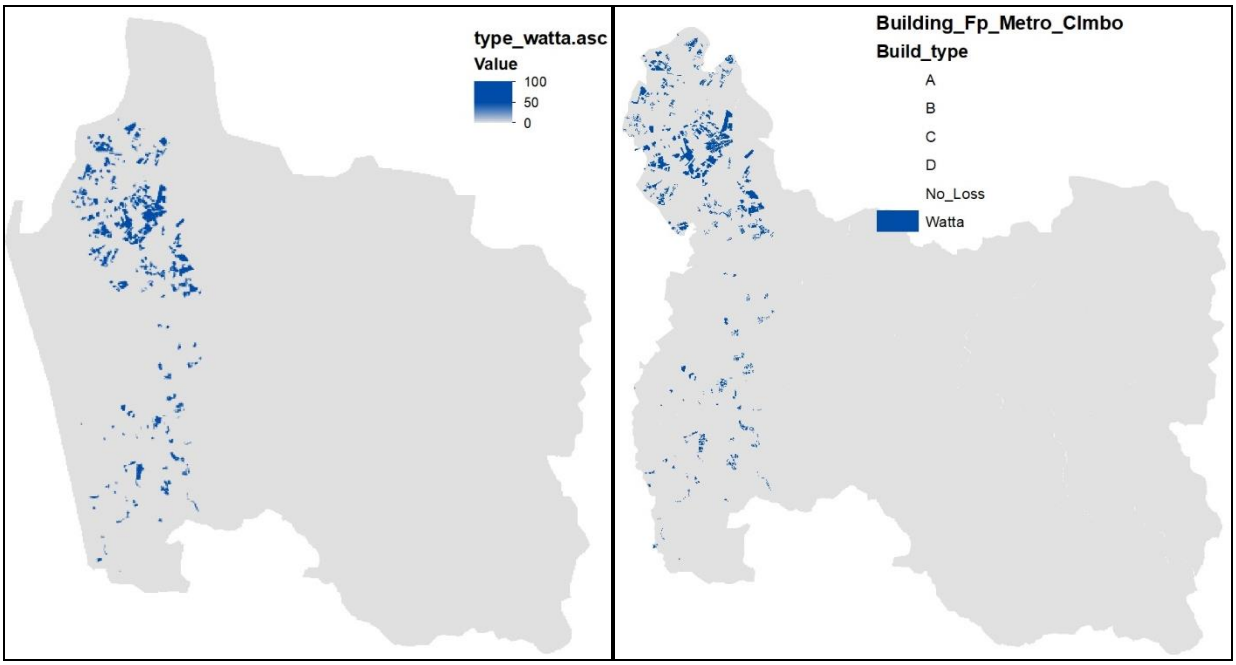
type_watta.asc
Value
100
50
0
Building_Fp_Metro_Clmbo
Build_type
A
B
C
D
No_Loss
Watta

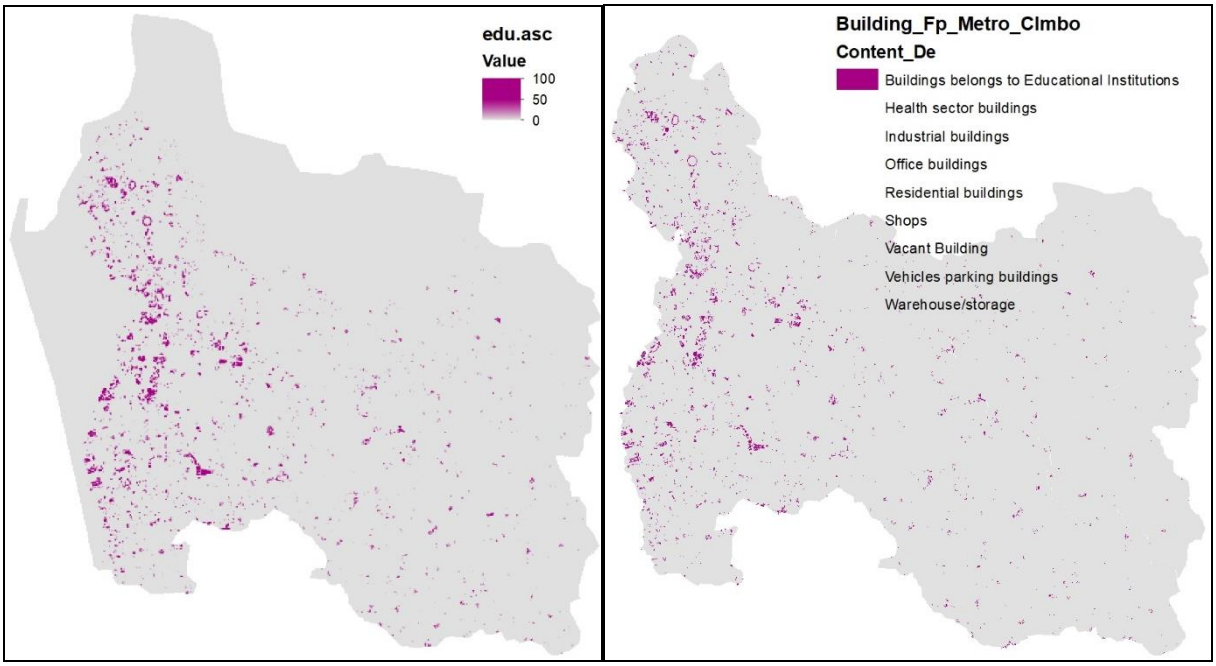
edu.asc
Value
100
50
0
Building_Fp_Metro_Clmbo
Content_De
Buildings belongs to Educational Institutions
Health sector buildings
Industrial buildings
Office buildings
Residential buildings
Shops
Vacant Building
Vehicles parking buildings
Warehouse/storage

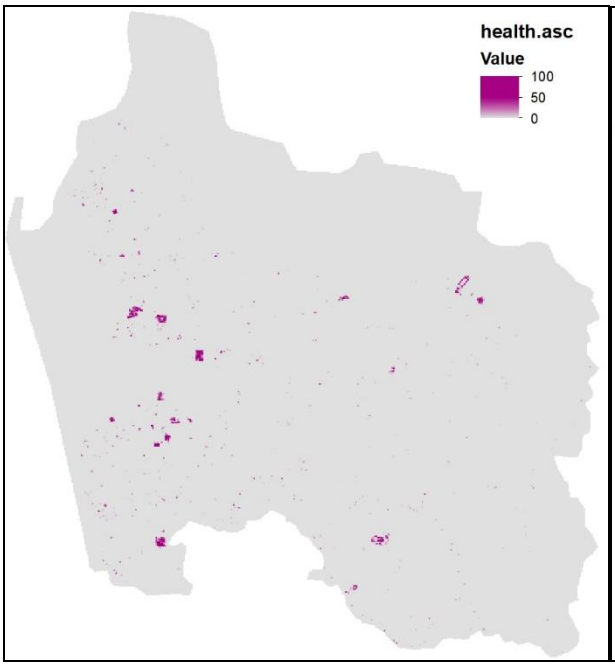
health.asc
Value
100
50
0

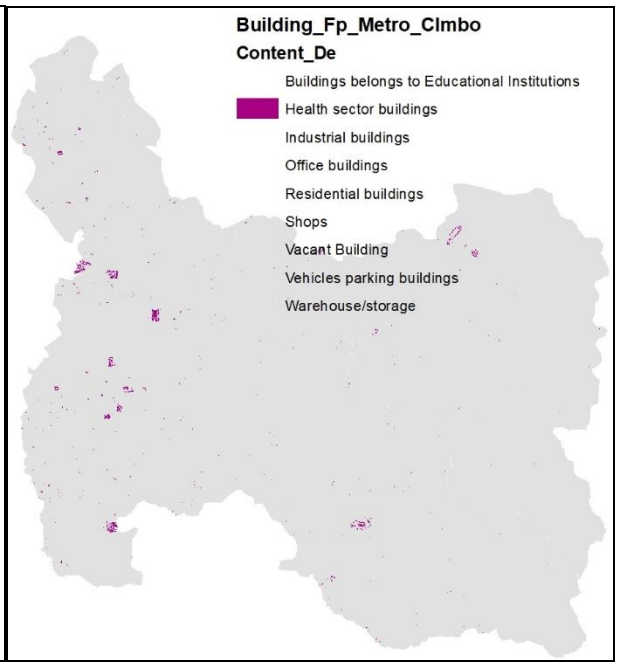
Building_Fp_Metro_Clmbo
Content_De
Buildings belongs to Educational Institutions
Health sector buildings
Industrial buildings
Office buildings
Residential buildings
Shops
Vacant Building
Vehicles parking buildings
Warehouse/storage

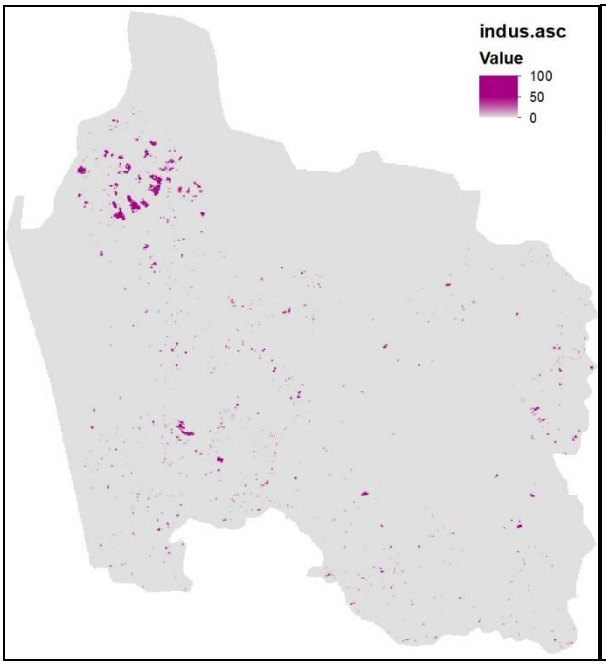
indus.asc
Value
100
50
0

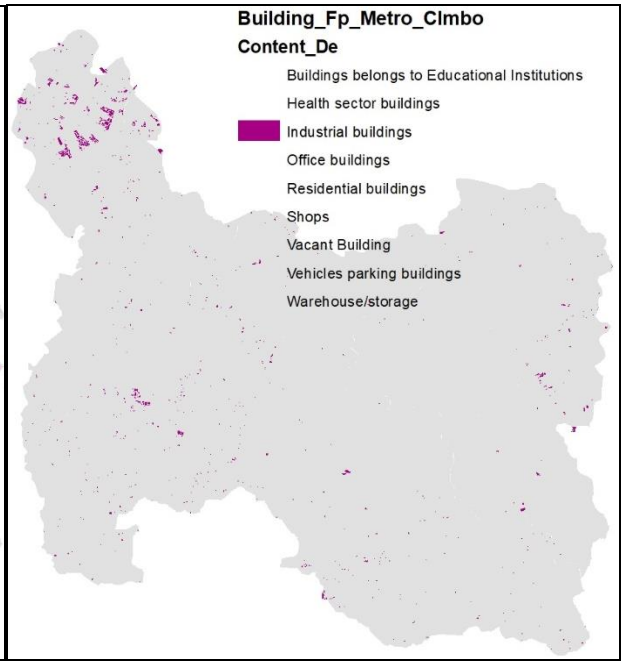
Building_Fp_Metro_Clmbo
Content_De
Buildings belongs to Educational Institutions
Health sector buildings
Industrial buildings
Office buildings
Residential buildings
Shops
Vacant Building
Vehicles parking buildings
Warehouse/storage

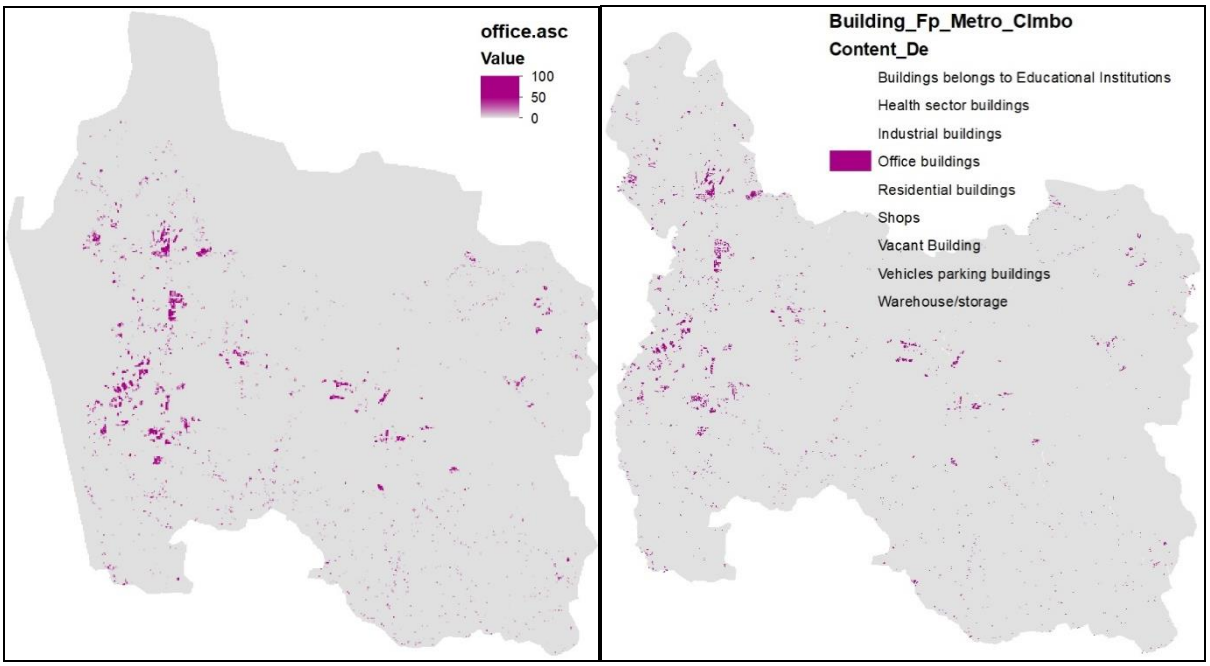
office.asc
Value
100
50
0
Building_Fp_Metro_Clmbo
Content_De
Buildings belongs to Educational Institutions
Health sector buildings
Industrial buildings
Office buildings
Residential buildings
Shops
Vacant Building
Vehicles parking buildings
Warehouse/storage


resid.asc
Value
100
50
0
Building_Fp_Metro_Clmbo
Content_De
Buildings belongs to Educational Institutions
Health sector buildings
Industrial buildings
Office buildings
Residential buildings
Shops
Vacant Building
Vehicles parking buildings
Warehouse/storage

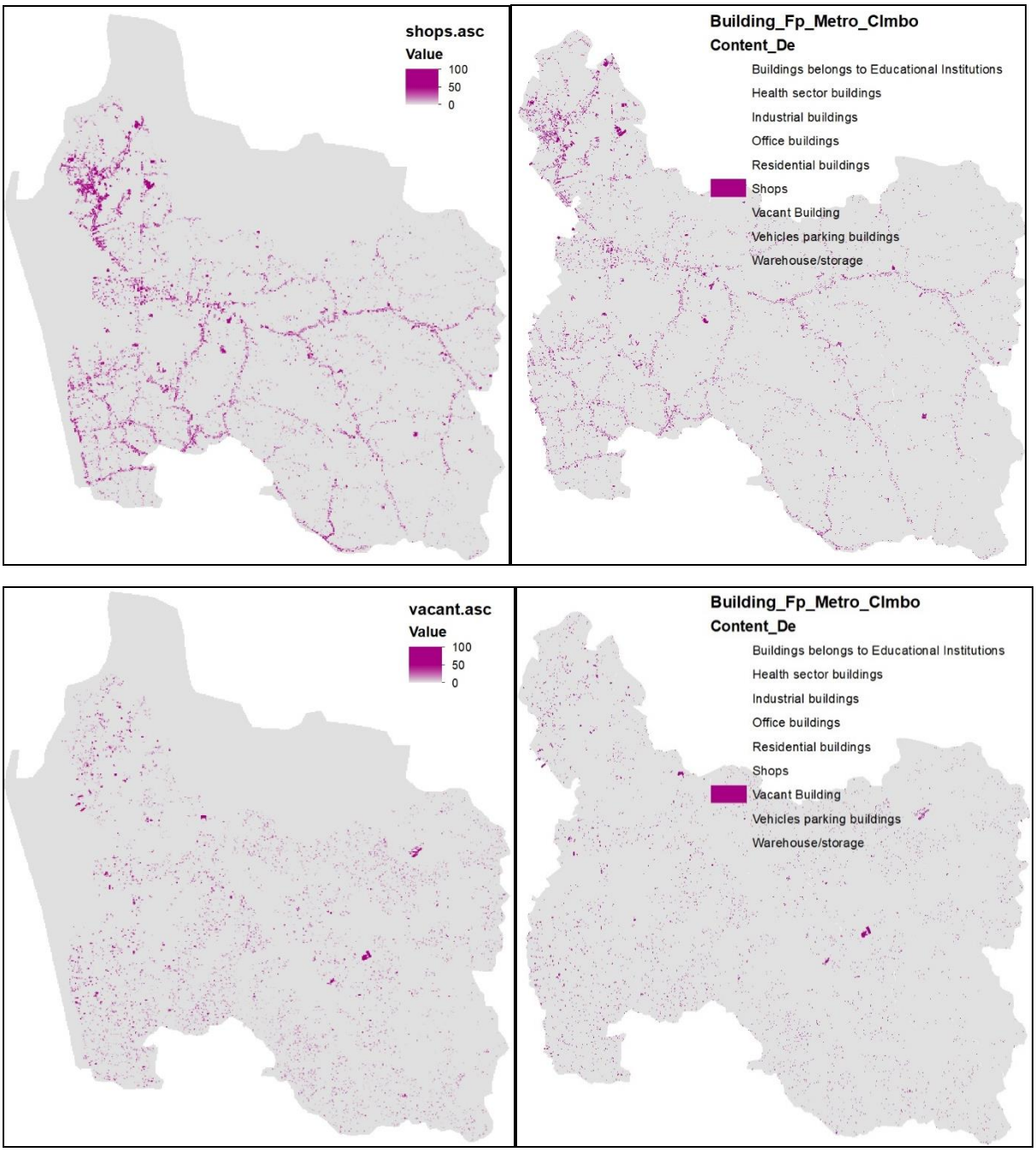
shops.asc
Value
100
50
0
Building_Fp_Metro_Clmbo
Content_De
Buildings belongs to Educational Institutions
Health sector buildings
Industrial buildings
Office buildings
Residential buildings
Shops
Vacant Building
Vehicles parking buildings
Warehouse/storage
vacant.asc
Value
100
50
0
Building_Fp_Metro_Clmbo
Content_De
Buildings belongs to Educational Institutions
Health sector buildings
Industrial buildings
Office buildings
Residential buildings
Shops
Vacant Building
Vehicles parking buildings
Warehouse/storage

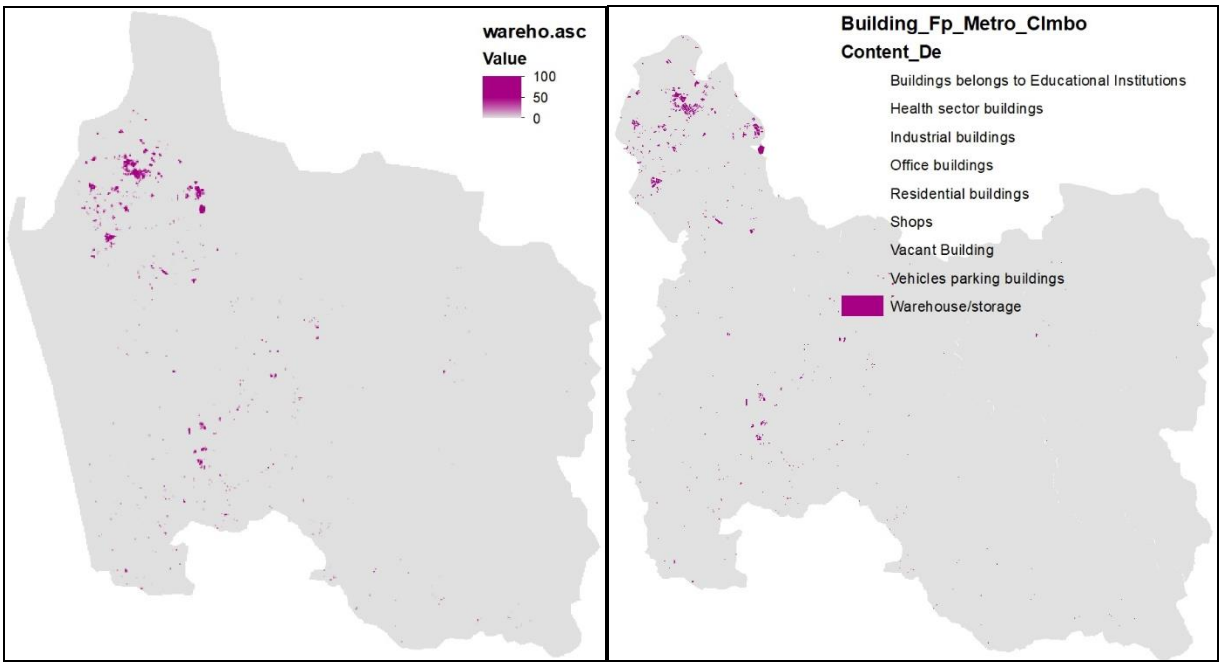
wareho.asc
Value
100
50
0
Building_Fp_Metro_Clmbo
Content_De
Buildings belongs to Educational Institutions
Health sector buildings
Industrial buildings
Office buildings
Residential buildings
Shops
Vacant Building
Vehicles parking buildings
Warehouse/storage

7.5. Annex 05 - Calculations for the comparisons between the vector and raster calculations.

Structural damage - Existing conditions - Vector calculations

Build_type	HK10	HK25	HK50	HK100	LK10	LK25	LK50	LK100
A (vector)	115,481,558	313,747,563	678,153,671	1,015,322,723	86,867,359	247,765,619	550,032,367	890,406,427
B (vector)	2,246,986,832	5,350,359,796	10,709,674,245	17,182,804,728	1,978,645,928	4,135,331,533	9,640,355,466	15,628,914,809
C (vector)	119,734,278	366,680,806	873,994,077	1,257,847,654	82,910,813	238,458,727	628,515,980	1,062,125,275
D (vector)	1,723,361,124	3,180,615,848	6,123,392,935	8,709,567,259	1,634,096,501	2,648,092,947	4,846,701,719	7,033,530,060
Watta (vector)	98,602,891	207,267,528	372,586,027	487,803,296	77,016,458	125,056,244	189,054,464	313,891,273
Total	4,304,166,684	9,418,671,541	18,757,800,957	28,653,345,661	3,859,537,059	7,394,705,070	15,854,659,995	24,928,867,844

Structural damage - Existing conditions - Raster calculations

Build_type	HK10	HK25	HK50	HK100	LK10	LK25	LK50	LK100
A (vector)	114,364,512	312,102,278	676,377,212	1,013,853,693	85,800,209	246,302,294	548,435,019	889,014,651
B (vector)	2,248,469,417	5,369,911,152	10,773,570,598	17,285,644,320	1,979,204,881	4,155,100,089	9,712,280,087	15,735,830,165
C (vector)	119,504,764	366,439,337	873,273,639	1,257,287,328	82,516,318	238,320,018	628,477,618	1,062,093,677
D (vector)	1,763,724,754	3,230,773,907	6,308,555,087	8,865,819,870	1,679,299,029	2,689,381,725	4,894,323,819	7,085,637,785
Watta (vector)	97,693,258	206,116,176	371,209,070	486,738,098	76,012,537	124,305,058	188,194,792	313,104,686
Total	4,343,756,704	9,485,342,851	19,002,985,605	28,909,343,309	3,902,832,974	7,453,409,183	15,971,711,336	25,085,680,964

Comparison of structural damage - Existing conditions -

Vector and raster calculations

	Vector	Raster	Difference	As a percentage
HK10	4,304,166,684	4,343,756,704	39,590,020	0.92%
HK25	9,418,671,541	9,485,342,851	66,671,309	0.71%
HK50	18,757,800,957	19,002,985,605	245,184,649	1.31%
HK100	28,653,345,661	28,909,343,309	255,997,648	0.89%
LK10	3,859,537,059	3,902,832,974	43,295,915	1.12%
LK25	7,394,705,070	7,453,409,183	58,704,113	0.79%
LK50	15,854,659,995	15,971,711,336	117,051,341	0.74%
LK100	24,928,867,844	25,085,680,964	156,813,120	0.63%

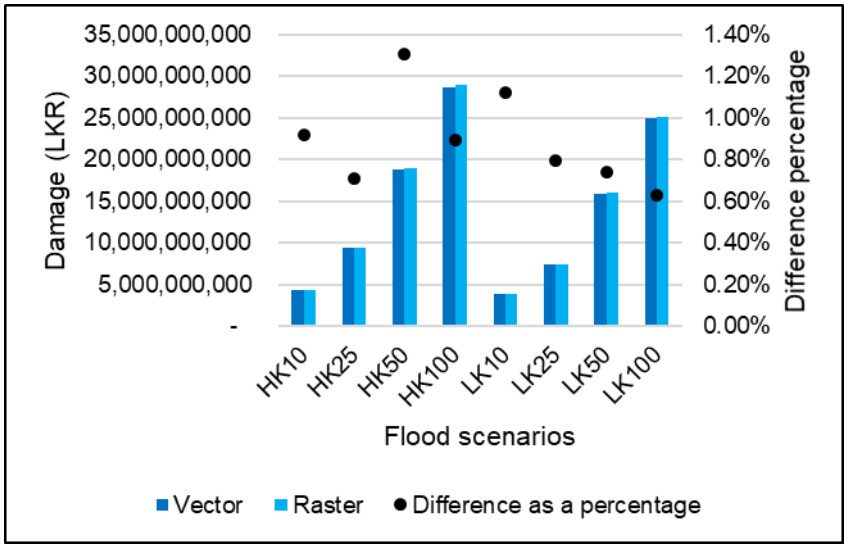

Content damage - Existing conditions - Vector calculations

Content_De	HK10	HK25	HK50	HK100	LK10	LK25	LK50	LK100
Educational	33,278,971	71,320,558	168,461,532	295,614,167	29,726,284	58,717,657	141,833,508	235,253,070
Health	35,673,128	77,857,561	142,957,714	246,923,149	35,997,628	74,195,409	135,073,475	221,373,283
Industrial	152,310,864	401,395,000	1,020,237,451	1,410,160,154	136,055,028	253,162,543	506,383,519	795,633,218
Office	309,992,114	601,891,456	1,212,278,657	2,092,323,928	311,724,186	520,529,131	1,085,878,299	1,905,245,359
Residential	604,469,659	1,562,435,086	3,464,085,547	5,490,882,767	515,894,826	1,087,270,046	2,555,069,569	4,533,536,702
Shops	72,362,103	145,612,452	366,300,382	616,394,154	78,003,890	116,297,798	268,960,076	498,901,040
Vacant	42,429,448	124,330,498	255,467,297	358,465,887	34,078,586	66,990,107	154,178,187	278,994,307
Warehouse	215,666,630	448,410,705	1,093,465,002	1,730,613,308	202,695,164	396,591,062	840,388,571	1,371,442,579
Total	1,466,182,917	3,433,253,316	7,723,253,583	12,241,377,514	1,344,175,592	2,573,753,753	5,687,765,204	9,840,379,558

Content damage - Existing conditions - Raster calculations

Content_De	HK10	HK25	HK50	HK100	LK10	LK25	LK50	LK100
Educational	33,659,401	71,327,816	168,373,463	295,589,783	30,044,223	58,770,590	141,922,523	235,354,945
Health	35,673,107	77,894,529	143,147,361	247,234,598	35,997,626	74,233,940	135,264,676	221,686,286
Industrial	170,401,541	424,773,255	1,107,053,173	1,475,564,659	167,240,531	266,342,018	522,998,496	816,119,173
Office	127,442,686	321,238,703	740,034,078	1,424,917,237	128,762,608	264,708,211	642,172,056	1,274,614,033
Residential	607,479,071	1,564,682,984	3,472,866,348	5,513,648,073	518,068,840	1,090,013,686	2,569,053,081	4,559,043,947
Shops	72,506,431	145,574,543	366,519,344	618,396,254	78,284,265	116,775,677	270,692,079	501,928,783
Vacant	42,915,380	124,445,811	256,033,891	359,692,702	34,685,477	67,009,849	154,416,187	279,944,196
Warehouse	223,513,440	459,170,103	1,242,361,067	1,821,426,121	209,780,893	407,456,302	851,812,150	1,382,820,074
Total	1,313,591,059	3,189,107,742	7,496,388,725	11,756,469,427	1,202,864,463	2,345,310,273	5,288,331,248	9,271,511,439

Comparison of content damage - Existing conditions -

Vector and raster calculations

	Vector	Raster	Difference	As a percentage
HK10	1,466,182,917	1,313,591,059	(152,591,859)	-10.41%
HK25	3,433,253,316	3,189,107,742	(244,145,574)	-7.11%
HK50	7,723,253,583	7,496,388,725	(226,864,858)	-2.94%
HK100	12,241,377,514	11,756,469,427	(484,908,087)	-3.96%
LK10	1,344,175,592	1,202,864,463	(141,311,129)	-10.51%
LK25	2,573,753,753	2,345,310,273	(228,443,480)	-8.88%

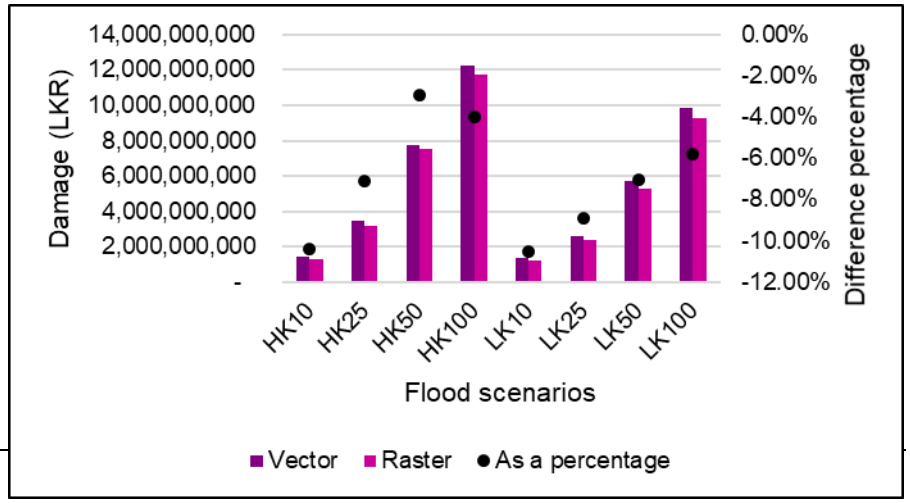

LK50	5,687,765,204	5,288,331,248	(399,433,957)	-7.02%
LK100	9,840,379,558	9,271,511,439	(568,868,120)	-5.78%

Structural damage - With all interventions - Vector calculations

Build_type	HK10	HK25	HK50	HK100	LK25	LK50	LK100
A (vector)	125,207,477	269,688,682	585,808,901	949,379,337	249,100,051	563,099,162	872,150,004
B (vector)	2,309,124,257	4,537,306,540	9,676,492,724	16,837,670,780	4,111,127,236	9,413,899,184	15,262,314,779
C (vector)	103,489,379	262,267,581	707,319,287	1,154,238,346	263,267,594	692,902,296	1,090,420,021
D (vector)	1,576,460,572	2,673,738,503	5,069,500,917	7,536,079,281	2,606,353,443	4,727,470,742	6,945,006,253
Watta (vector)	75,256,107	124,695,337	241,842,831	333,584,083	111,501,451	182,138,673	288,743,568
Total	4,189,537,792	7,867,696,644	16,280,964,661	26,810,951,827	7,341,349,776	15,579,510,057	24,458,634,624

Structural damage - With all interventions - Raster calculations

Build_type	HK10	HK25	HK50	HK100	LK25	LK50	LK100
A (vector)	124,191,414	268,173,155	584,086,366	947,924,423	247,673,459	561,456,962	870,803,034
B (vector)	2,308,234,632	4,555,786,880	9,739,617,605	16,942,231,410	4,132,435,302	9,480,784,890	15,366,895,110
C (vector)	103,283,789	262,010,745	706,548,279	1,153,578,404	263,229,873	692,728,928	1,090,408,099
D (vector)	1,615,419,941	2,723,666,745	5,262,959,605	7,714,315,976	2,647,364,456	4,777,352,597	6,996,747,761
Watta (vector)	74,545,195	123,696,429	240,416,848	332,286,065	110,816,036	181,242,942	287,942,681
Total	4,225,674,972	7,933,333,955	16,533,628,704	27,090,336,279	7,401,519,126	15,693,566,320	24,612,796,685

Comparison of structural damage - With all interventions -

Vector and raster calculations

	Vector	Raster	Difference	As a percentage
HK10	4,189,537,792	4,225,674,972	36,137,179	0.86%
HK25	7,867,696,644	7,933,333,955	65,637,312	0.83%
HK50	16,280,964,661	16,533,628,704	252,664,042	1.55%
HK100	26,810,951,827	27,090,336,279	279,384,451	1.04%
LK25	7,341,349,776	7,401,519,126	60,169,350	0.82%
LK50	15,579,510,057	15,693,566,320	114,056,262	0.73%
LK100	24,458,634,624	24,612,796,685	154,162,061	0.63%

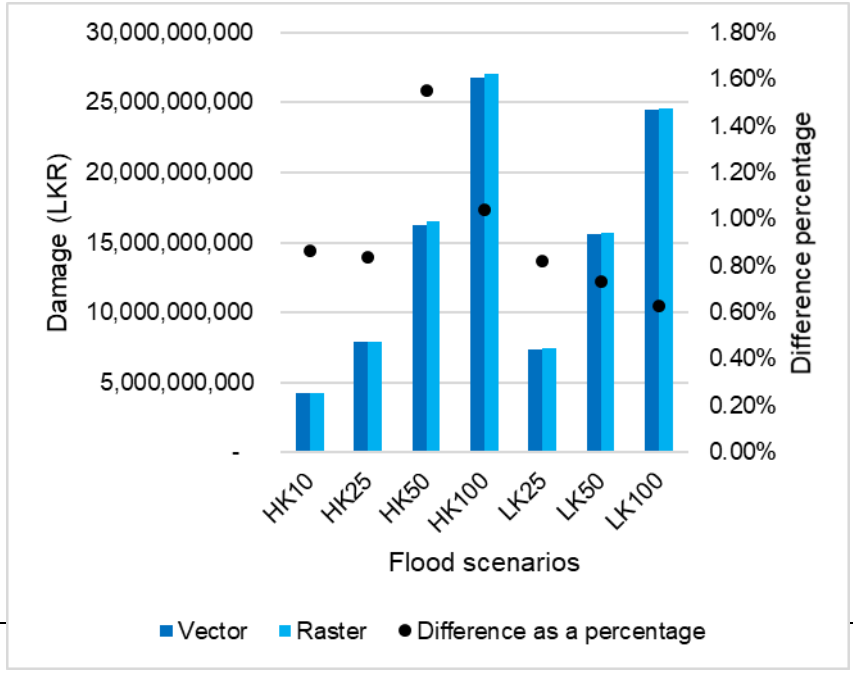

Content damage - With all interventions - Vector calculations

Content_De	HK10	HK25	HK50	HK100	LK25	LK50	LK100
Educational	31,342,075	59,727,995	132,092,170	256,473,332	60,705,931	136,952,134	234,405,485
Health	35,422,883	73,563,750	132,643,095	226,796,487	74,470,984	134,999,072	228,839,907
Industrial	127,882,098	255,079,009	659,141,389	895,273,661	238,937,297	468,945,565	793,856,662
Office	325,865,409	548,657,272	1,086,340,876	2,037,185,141	525,185,093	1,062,182,270	1,892,497,097
Residential	593,934,320	1,195,575,756	2,805,758,618	4,974,059,689	1,074,062,103	2,553,267,315	4,435,657,336
Shops	66,632,903	122,861,133	314,649,877	559,339,934	112,700,222	263,316,149	488,872,055
Vacant	47,735,453	84,807,437	208,652,649	328,615,261	64,747,187	156,999,774	268,197,267
Warehouse	182,049,376	378,785,808	846,467,769	1,427,750,058	380,344,975	800,370,107	1,352,196,621
Total	1,410,864,518	2,719,058,159	6,185,746,443	10,705,493,563	2,531,153,792	5,577,032,386	9,694,522,429

Content damage - With all interventions - Raster calculations

Content_De	HK10	HK25	HK50	HK100	LK25	LK50	LK100
Educational	31,638,500	59,740,303	132,016,861	256,432,610	60,753,408	137,037,708	234,503,945
Health	35,422,861	73,591,472	132,824,997	227,118,724	74,504,884	135,179,469	229,151,362
Industrial	142,855,340	278,795,172	749,692,662	974,435,893	252,078,680	486,942,306	814,304,491
Office	142,478,804	280,494,170	643,858,564	1,386,604,870	260,388,098	621,807,597	1,267,479,787
Residential	596,529,364	1,197,339,026	2,815,077,618	4,997,803,042	1,076,912,822	2,565,714,926	4,460,648,655
Shops	66,893,987	122,855,889	314,725,804	561,229,892	113,126,543	264,937,132	491,848,444
Vacant	48,192,190	84,929,106	209,208,595	329,930,084	64,766,929	157,178,507	269,140,698
Warehouse	190,138,094	389,180,734	1,020,061,815	1,555,981,081	391,210,372	811,714,615	1,363,565,408
Total	1,254,149,140	2,486,925,872	6,017,466,916	10,289,536,196	2,293,741,735	5,180,512,260	9,130,642,791

Comparison of content damage - With all interventions -

Vector and raster calculations

	Vector	Raster	Difference	As a percentage
HK10	1,410,864,518	1,254,149,140	(156,715,377)	-11.11%
HK25	2,719,058,159	2,486,925,872	(232,132,287)	-8.54%
HK50	6,185,746,443	6,017,466,916	(168,279,527)	-2.72%
HK100	10,705,493,563	10,289,536,196	(415,957,367)	-3.89%
LK25	2,531,153,792	2,293,741,735	(237,412,057)	-9.38%
LK50	5,577,032,386	5,180,512,260	(396,520,126)	-7.11%
LK100	9,694,522,429	9,130,642,791	(563,879,638)	-5.82%

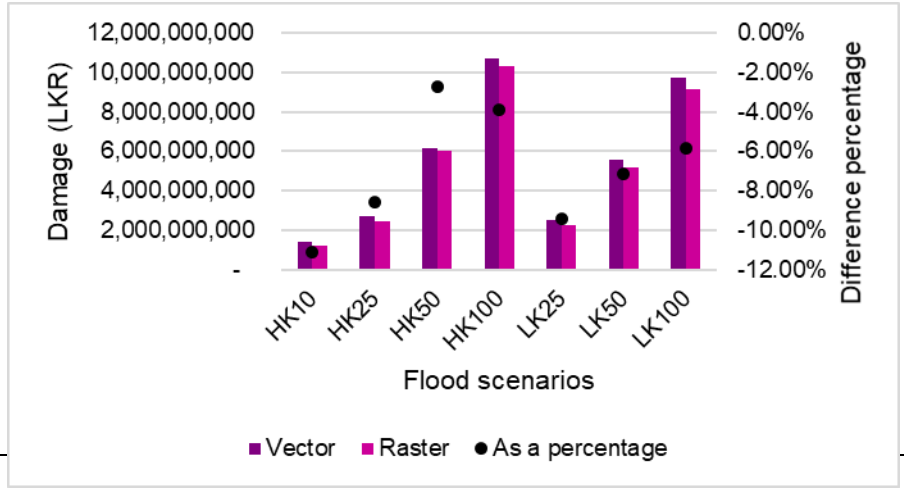

7.6. Annex 06 - Comparison of three methods to project the content damage of the residential buildings

30 m Existing conditions

Return period of the floods	10	25	50	100
HK-PHRD (25% of the structural damage)	645,192,219	1,559,513,923	3,158,597,257	4,985,934,381
HK-60% of the structural damage	1,548,461,326	3,742,833,416	7,580,633,417	11,966,242,514
HK-By Content Damage Function	604,469,659	1,562,435,086	3,464,085,547	5,490,882,767
LK-PHRD (25% of the structural damage)	556,360,140	1,186,653,031	2,751,987,909	4,473,825,029
LK-60% of the structural damage	1,335,264,335	2,847,967,274	6,604,770,981	10,737,180,069
LK-By Content Damage Function	515,894,826	1,087,270,046	2,555,069,569	4,533,536,702

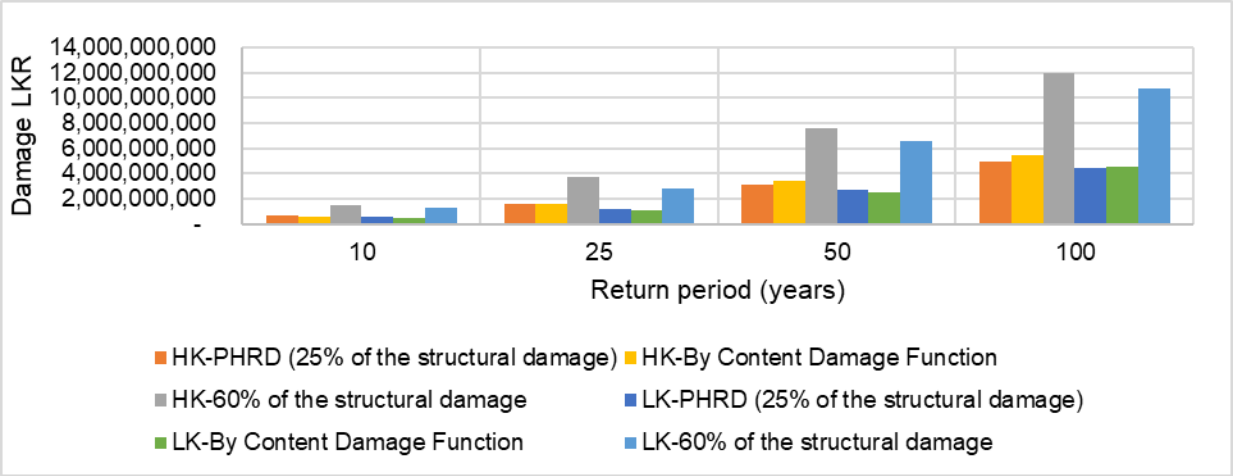

30 m with all interventions

Return period of the floods	10	25	50	100
HK-PHRD (25% of the structural damage)	653,261,585	1,298,487,875	2,802,862,570	4,818,707,096
HK-60% of the structural damage	1,567,827,803	3,116,370,899	6,726,870,169	11,564,897,030
HK-By Content Damage Function	593,934,320	1,195,575,756	2,805,758,618	4,974,059,689
LK-PHRD (25% of the structural damage)	-	1,183,747,423	2,713,009,829	4,378,399,764
LK-60% of the structural damage	-	2,840,993,815	6,511,223,589	10,508,159,434
LK-By Content Damage Function	-	1,074,062,103	2,553,267,315	4,435,657,336

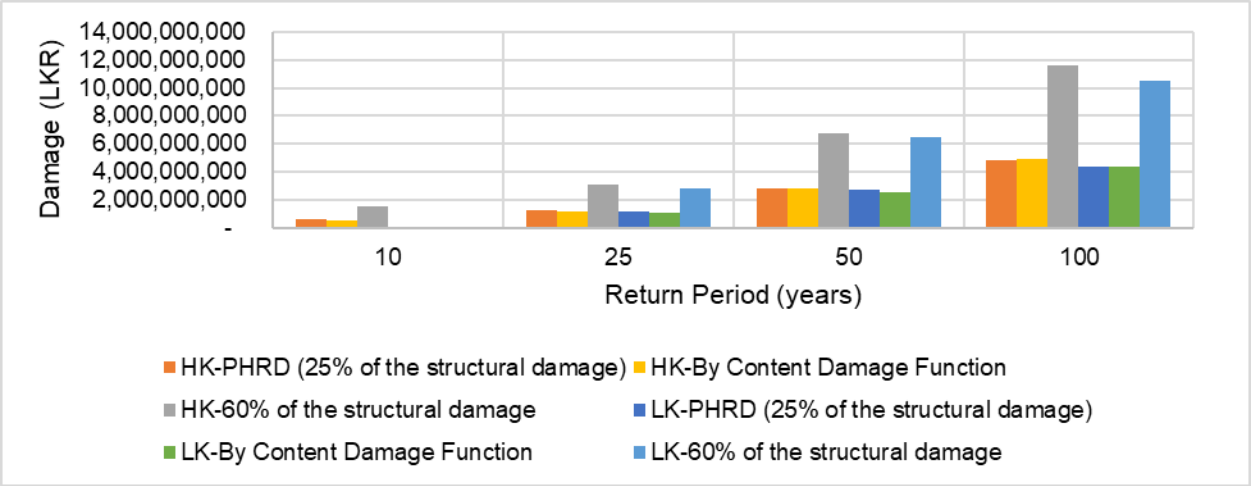

From the results, it could be seen that the damage values obtained by the content damage functions and by the 25% of the structural value are very similar, therefore the cluster 2 damage functions could be used for the estimation of the content damages. This factor is furthermore supported by the following table.

Existing conditions	25% of the content damage	Damage Curve (cluster 2)	Difference	As a percentage
HK10	604,469,659	645,192,219	(40,722,560)	-6.31%
HK25	1,562,435,086	1,559,513,923	2,921,163	0.19%
HK50	3,464,085,547	3,158,597,257	305,488,290	9.67%
HK100	5,490,882,767	4,985,934,381	504,948,387	10.13%
LK10	556,360,140	515,894,826	40,465,314	7.84%
LK25	1,186,653,031	1,087,270,046	99,382,985	9.14%
LK50	2,751,987,909	2,555,069,569	196,918,340	7.71%
LK100	4,473,825,029	4,533,536,702	(59,711,673)	-1.32%

With all interventions	25% of the content damage	Damage Curve (cluster 2)	Difference	As a percentage
HK10	653,261,585	593,934,320	59,327,265	9.99%
HK25	1,298,487,875	1,195,575,756	102,912,119	8.61%
HK50	2,802,862,570	2,805,758,618	(2,896,048)	-0.10%
HK100	4,818,707,096	4,974,059,689	(155,352,593)	-3.12%
LK25	1,183,747,423	1,074,062,103	109,685,320	10.21%
LK50	2,713,009,829	2,553,267,315	159,742,513	6.26%
LK100	4,378,399,764	4,435,657,336	(57,257,571)	-1.29%

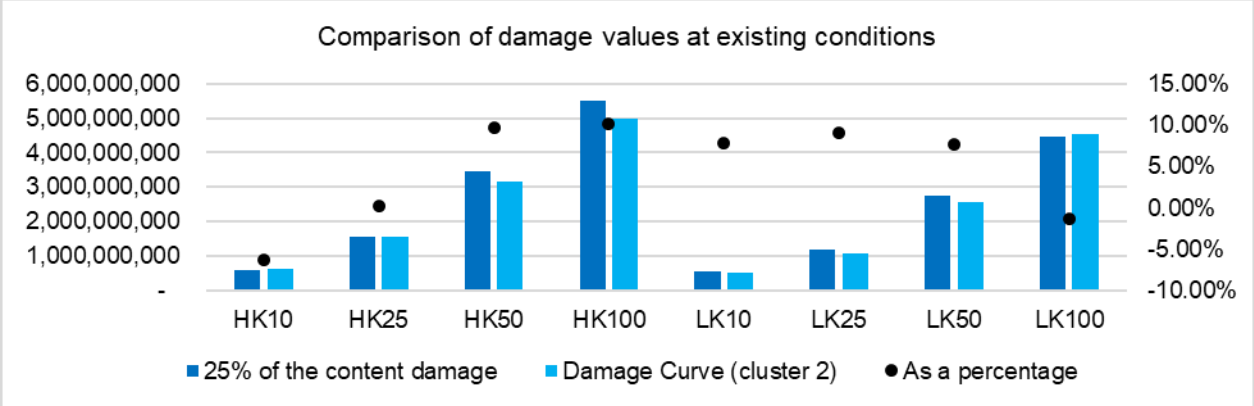

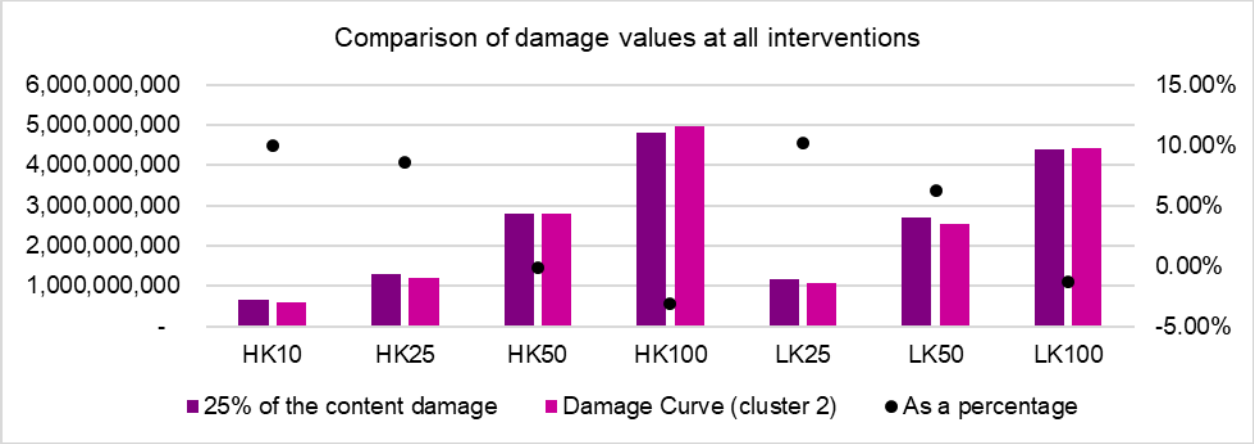
Comparison of damage values at all interventions
6,000,000,000
5,000,000,000
4,000,000,000
3,000,000,000
2,000,000,000
1,000,000,000
-
15.00%
10.00%
5.00%
0.00%
-5.00%
HK10
HK25
HK50
HK100
LK25
LK50
LK100
25% of the content damage
Damage Curve (cluster 2)
As a percentage